

# Interpreting a 750 GeV Diphoton Resonance

---

Rick S. Gupta,<sup>a</sup> Sebastian Jäger,<sup>a,b</sup> Yevgeny Kats,<sup>a</sup> Gilad Perez,<sup>a</sup> Emmanuel Stamou<sup>a</sup>

<sup>a</sup>*Department of Particle Physics and Astrophysics, Weizmann Institute of Science,  
Rehovot 7610001, Israel*

<sup>b</sup>*Department of Physics and Astronomy, University of Sussex,  
Brighton, BN1 9QH, UK*

*E-mail:* [rsgupta@weizmann.ac.il](mailto:rsgupta@weizmann.ac.il), [S.Jaeger@sussex.ac.uk](mailto:S.Jaeger@sussex.ac.uk),  
[yevgeny.kats@weizmann.ac.il](mailto:yevgeny.kats@weizmann.ac.il), [gilad.perez@weizmann.ac.il](mailto:gilad.perez@weizmann.ac.il),  
[emmanuel.stamou@weizmann.ac.il](mailto:emmanuel.stamou@weizmann.ac.il)

**ABSTRACT:** We discuss the implications of the significant excesses in the diphoton final state observed by the LHC experiments ATLAS and CMS around a diphoton invariant mass of 750 GeV. The interpretation of the excess as a spin-zero  $s$ -channel resonance implies model-independent lower bounds on both its branching ratio and its coupling to photons, which stringently constrain dynamical models. We consider both the case where the excess is described by a narrow and a broad resonance. We also obtain model-independent constraints on the allowed couplings and branching fractions to final states other than diphotons, by including the interplay with 8 TeV searches. These results can guide attempts to construct viable dynamical models of the resonance. Turning to specific models, our findings suggest that the anomaly cannot be accounted for by the presence of only an additional singlet or doublet spin-zero field and the Standard Model degrees of freedom; this includes all two-Higgs-doublet models. We prove that the whole parameter space of the MSSM is ruled out as an explanation for the excess if stability of the electroweak vacuum is required. If we assume that the resonance is broad we find that it is challenging to find a weakly coupled explanation. However, we provide an existence proof in the form of a model with vectorlike quarks with exotic electric charge of  $5/3$  or above. For the narrow-resonance case a similar model can be perturbative up to high scales also with smaller charges. We also consider dilaton models; they appear to be challenged by the data, even if arbitrary extra contributions to the QED and QCD beta functions are allowed. Some implications for flavor physics are briefly discussed.

---

## Contents

<b>1</b>	<b>Introduction</b>	<b>1</b>
<b>2</b>	<b>Model-independent constraints</b>	<b>2</b>
2.1	Implications of the excess alone	2
2.2	Interplay with previous LHC searches	6
<b>3</b>	<b>Models</b>	<b>9</b>
3.1	SM-singlet scalar	10
3.1.1	Renormalizable model	10
3.1.2	Boosting $c_\gamma, c_g$ with new vectorlike fermions	11
3.1.3	The dilaton	13
3.1.4	A pseudoscalar	15
3.2	Excluding the general pure 2HDM	16
3.3	The fate of the MSSM	19
3.3.1	Constraints from vacuum stability	21
3.3.2	Conservative bounds on sfermion contributions	22
3.3.3	Contributions from other particles and verdict	23
<b>4</b>	<b>Summary and Outlook</b>	<b>24</b>

---

## 1 Introduction

Very recently, both the ATLAS and the CMS collaborations at CERN have reported mutually consistent “bumps” in the diphoton invariant mass distribution around 750 GeV [1, 2]. Based on 3.2 and 2.6 fb<sup>-1</sup> of the 13 TeV LHC data, the corresponding deviations from the background-only hypothesis have a local significance of 3.9 $\sigma$  and 2.6 $\sigma$  in ATLAS and CMS, respectively. The bumps are best described by a relative width  $\Gamma/M \approx 6\%$  in ATLAS [1] but a sub-resolution width in CMS [2], with the discrepancy likely arising due to statistical fluctuations. The resonant excesses are suggestive of the decay of a new particle beyond the Standard Model (BSM). The kinematic properties of the events in the excess region are reported not to show significant deviations compared with events in sidebands. This disfavors significant contributions to the production from decays of yet heavier particles or associated production and motivates focusing on the case of a single production of a 750 GeV resonance.

The purpose of the present paper is to characterise this theoretically unexpected result and discuss its implications for some leading paradigms for physics beyond the Standard Model. It is divided into two main parts, the first of which comprises a model-independent framework that aims to equip the reader with handy formulas for interpreting both the

signal and the most important resonance search constraints from existing LHC searches in the context of BSM models. We derive a number of bounds, including model-independent lower bounds on the branching ratio and partial width into photons of the hypothetical new particle. The second part investigates concrete scenarios, including the possibility of interpreting the resonance as the dilaton of theories with spontaneous breaking of scale invariance or as a heavy Higgs scalar in two-Higgs-doublet models (2HDM). We find the properties of the observed resonance to be quite constraining. In particular, the interpretation as an  $s$ -channel resonance, if confirmed, cannot be accommodated within the Minimal Supersymmetric Standard Model (MSSM) even under the most conservative assumptions about the MSSM parameters and the true width of the resonance; this conclusion holds if we require the absence of charge- and colour-breaking minima.

## 2 Model-independent constraints

We start by discussing what can be inferred about the new particle from data alone. We will first describe the implications of the observed properties of the diphoton bumps, and then examine the constraints from the absence of significant excesses in resonance searches in other final states that could be sensitive to other decay modes of the same particle.

### 2.1 Implications of the excess alone

Both ATLAS and CMS observe excesses in a diphoton invariant mass region near 750 GeV [1, 2]. For the purposes of this work, we will generally assume the signal contribution to be  $N = 20$  events for  $\mathcal{L} = 5.8 \text{ fb}^{-1}$  integrated luminosity (adding up ATLAS and CMS), but will make clear the scaling of our findings with  $N$  wherever feasible. We will assume a signal efficiency (including acceptance) of  $\epsilon = 50\%$ , even though, in general, this does have some dependence on both the experiment and the details of the signal model.

The most straightforward signal interpretation is resonant  $s$ -channel production of a new unstable particle. The observed signal strength corresponds to a 13 TeV inclusive cross section to diphotons of

$$\sigma_{13} \times \text{BR}_{\gamma\gamma} \approx 6.9 \text{ fb} \times \left(\frac{N}{20}\right) \left(\frac{50\%}{\epsilon}\right) \left(\frac{5.8 \text{ fb}^{-1}}{\mathcal{L}_{13}}\right). \quad (2.1)$$

The diphoton final state precludes a spin-one interpretation due to the Landau-Yang theorem [3, 4], and we will henceforth assume spin zero. We take the mass to be  $M = 750 \text{ GeV}$ ; small variations have no significant impact on our findings. The shape of the excess in ATLAS may indicate a width of about  $\Gamma = 45 \text{ GeV}$  [1]. However, we will also contemplate the case of smaller width below, and discuss how our main findings depend on this.

A minimal dynamical input is necessary to interpret the result and incorporate 8 TeV LHC constraints. The width-to-mass ratio is small enough to justify a narrow-width approximation to the level of accuracy we aim at here. In the narrow-width limit, resonant scattering amplitudes factorize into production and decay vertices, which we parameterize

mode	Width coefficient $n_i$	$n_i$ (#)
$\gamma\gamma$	$\frac{1}{16(4\pi)^5}$	$1.99 \times 10^{-7}$
$gg$	$\frac{1}{2(4\pi)^5}$	$1.60 \times 10^{-6}$
$q_i\bar{q}_i$	$\frac{3}{8\pi}$	0.119
$t\bar{t}$	$\frac{3}{8\pi}\sqrt{1-4m_t^2/M^2}$	0.106
$W^+W^-$	$\frac{1}{64\pi}\sqrt{1-4m_W^2/M^2}\frac{M^2}{m_W^2}\left[1-4\frac{m_W^2}{M^2}+12\frac{m_W^4}{M^4}\right]$	0.404
$ZZ$	$\frac{1}{128\pi}\sqrt{1-4m_Z^2/M^2}\frac{M^2}{m_Z^2}\left[1-4\frac{m_Z^2}{M^2}+12\frac{m_Z^4}{M^4}\right]$	0.154

**Table 1.** Width coefficients.

by terms in a ‘‘Lagrangian’’ for the resonance  $\mathcal{S}$ ,

$$\mathcal{L} = -\frac{1}{16\pi^2}\frac{1}{4}\frac{c_\gamma}{M}\mathcal{S}F^{\mu\nu}F_{\mu\nu} - \frac{1}{16\pi^2}\frac{1}{4}\frac{c_g}{M}\mathcal{S}G^{\mu\nu,a}G_{\mu\nu}^a - c_W M_W \mathcal{S}W^{+\mu}W_\mu^- - \frac{1}{2}c_Z M_Z \mathcal{S}Z^\mu Z_\mu - \sum_f c_f \mathcal{S}\bar{f}f. \quad (2.2)$$

In this parametrization,  $M$  is the mass of the resonance  $\mathcal{S}$ . We emphasize that each term denotes a particular production and/or decay vertex and that the parameterization  $\mathcal{L}$  does not make any assumptions about hierarchies of scales.<sup>1</sup> Note that if  $\mathcal{S}$  is a pseudoscalar, one should set  $c_W = c_Z = 0$  and replace  $F^{\mu\nu}F_{\mu\nu} \rightarrow F^{\mu\nu}\tilde{F}_{\mu\nu}$ ,  $G^{\mu\nu,a}G_{\mu\nu}^a \rightarrow G^{\mu\nu,a}\tilde{G}_{\mu\nu}^a$ ,  $\mathcal{S}\bar{f}f \rightarrow i\mathcal{S}\bar{f}\gamma^5 f$  and all our results involving the couplings  $c_\gamma$ ,  $c_g$  and  $c_f$  would be applicable.

The total decay width of  $\mathcal{S}$  imposes one constraint on the couplings,

$$\frac{\Gamma}{M} = \sum_i \frac{\Gamma_i}{M} = \sum_i n_i |c_i|^2 \approx 0.06, \quad (2.3)$$

with the dimensionless coefficients  $n_i$  that will be useful to us listed in Table 1. In particular, Eq. (2.3) directly implies upper bounds on the magnitude of each  $c_i$ , since observations imply that the width cannot significantly exceed 45 GeV.

It is possible and convenient to represent the observed signal in terms of the branching ratios to the production mode and to  $\gamma\gamma$ . If a single production mode,  $p$ , dominates, the number of signal events,  $N$ , in the 13 TeV analyses fixes the product

$$\text{BR}_{\gamma\gamma} \times \text{BR}_p = n_p \frac{M}{\Gamma} \frac{N}{\epsilon x_S^{13,p} \mathcal{L}_{13}} = \kappa_p \times \left(\frac{N}{20}\right) \left(\frac{45 \text{ GeV}}{\Gamma}\right) \left(\frac{5.8 \text{ fb}^{-1}}{\mathcal{L}_{13}}\right), \quad (2.4)$$

where

$$\kappa_p \approx \{2.5, 5.5, 8.9, 96, 140, 310, 20000, 25000\} \times 10^{-5} \quad (2.5)$$

<sup>1</sup>In particular, the ‘‘couplings’’  $c_i$  are on-shell form factors that generally include contributions from light particles and CP-even phases due to unitarity cuts. Contributions from particles with mass  $\gg M$  can be matched to a local effective Lagrangian similar to Eq. (2.2). We discuss examples in Section 3.

$\sqrt{s}$	[pb]	$gg$	$u\bar{u}$	$d\bar{d}$	$s\bar{s}$	$c\bar{c}$	$b\bar{b}$	VBF $_{WW}$	VBF $_{ZZ}$
13	$x_{\mathcal{S}}^{13,p}$	$7.5 \cdot 10^{-3}$	250	150	14	9.8	4.4	0.23	$7.0 \cdot 10^{-2}$
8	$x_{\mathcal{S}}^{8,p}$	$1.7 \cdot 10^{-3}$	95	57	3.7	2.3	0.96	$5.5 \cdot 10^{-2}$	$1.7 \cdot 10^{-2}$
13/8	$r_p$	4.4	2.6	2.7	3.9	4.2	4.6	4.2	4.2

**Table 2.** Leading-order production cross sections for a resonance with  $M = 750$  GeV for  $c_g = c_f = c_\gamma = c_W = c_Z = 1$ , at the 13 TeV and 8 TeV LHC, and their ratio,  $r_p$ , using the leading-order PDF set `nn231o1` [9]. For the modes  $gg$ ,  $u\bar{u}$ ,  $d\bar{d}$ ,  $s\bar{s}$ ,  $c\bar{c}$ , and  $b\bar{b}$  the production cross section corresponds to the process  $pp \rightarrow \mathcal{S}$ ; for VBF $_{WW}$  and VBF $_{ZZ}$  to the process  $pp \rightarrow \mathcal{S}+jj$ .

for the production modes

$$p = gg, u\bar{u}, d\bar{d}, s\bar{s}, c\bar{c}, b\bar{b}, \text{VBF}_{WW}, \text{VBF}_{ZZ}, \quad (2.6)$$

respectively, with  $n_p = n_{gg}, n_{q_i\bar{q}_i}, n_{WW}, n_{ZZ}$  provided in Table 1.<sup>2</sup> We used the leading-order  $\sqrt{s} = 13$  TeV production cross sections for  $M = 750$  GeV,

$$\sigma_{13} = |c_p|^2 x_{\mathcal{S}}^{13,p}, \quad (2.7)$$

where  $x_{\mathcal{S}}^{13,p}$  are listed in Table 2. A direct consequence of Eq. (2.4) is a lower bound on the branching ratio into photons,

$$\text{BR}_{\gamma\gamma} > \kappa_p \left( \frac{N}{20} \right) \left( \frac{45 \text{ GeV}}{\Gamma} \right) \left( \frac{5.8 \text{ fb}^{-1}}{\mathcal{L}_{13}} \right). \quad (2.8)$$

Note that this bound becomes more stringent if the width of the resonance is reduced.

Alternatively, the excess events fix the product of couplings

$$|c_\gamma c_p| = \sqrt{n_\gamma^{-1} \frac{\Gamma}{M} \frac{N}{\epsilon x_{\mathcal{S}}^{13,p} \mathcal{L}_{13}}} = \rho_p \times \sqrt{\left( \frac{N}{20} \right) \left( \frac{\Gamma}{45 \text{ GeV}} \right) \left( \frac{5.8 \text{ fb}^{-1}}{\mathcal{L}_{13}} \right)}, \quad (2.9)$$

where

$$\rho_p \approx \{530, 2.9, 3.7, 12, 15, 22, 95, 170\}. \quad (2.10)$$

Importantly, increasing the production couplings,  $c_p$ , increases also the decay rates to the production modes. Since these compete with the  $\gamma\gamma$  decay,  $c_\gamma$  cannot be arbitrarily small. The smallest possible  $|c_\gamma|$  corresponds to the situation where the total width is dominated by the production mode (which in particular implies  $\Gamma_{\gamma\gamma} \ll \Gamma_p$ ). Since the dependence on  $|c_p|^2$  cancels between the production cross section and the diphoton branching

<sup>2</sup>Results for VBF production, here and below, involve the use of the  $\mathcal{S}WW$  and  $\mathcal{S}ZZ$  vertices in Eq. (2.2) in Madgraph [5]. This is correct in either of the following two situations: (i) the origin of the vertices is local physics, originating in scales  $\gg M$ , such as in the dilation case in Section 3.1.3; in such a case the vertices can be interpreted as a unitary-gauge Lagrangian couplings and be used off shell; or (ii) the production process is dominated by nearly on-shell  $W, Z$  bosons (the same prerequisite under which the equivalent-boson approximation [6, 7] is justified). VBF production of the 750 GeV resonance is also studied in Ref. [8].

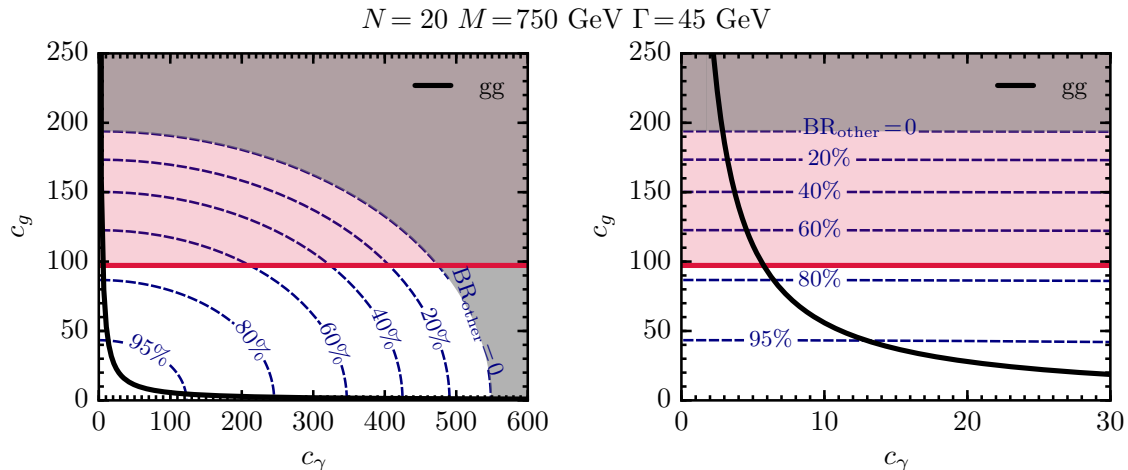


**Figure 1.** Black lines correspond to  $N = 20$  signal events in the diphoton analyses for  $M = 750$  GeV and  $\Gamma = 45$  GeV when the resonance is produced from  $gg$ . Blue dashed lines are contours of fixed branching ratio to modes other than  $\gamma\gamma$  or  $gg$ . The red-shaded area above the thick horizontal line is excluded by dijet resonance searches due to decays to  $gg$  alone. The shaded gray region corresponds to values of  $c_g, c_\gamma$  that produce a width larger than 45 GeV. The right panel is a blowup of the left one.

fraction in this limit, this bound is independent of  $\Gamma$ . We hence have the following model-independent lower bounds on  $c_\gamma$ :

$$|c_\gamma| > \sqrt{\frac{n_p}{n_\gamma} \frac{N}{\epsilon x_S^{13,p} \mathcal{L}_{13}}} = \{2.7, 4.1, 5.2, 17, 20, 30, 250, 280\} \times \sqrt{\left(\frac{N}{20}\right) \left(\frac{5.8 \text{ fb}^{-1}}{\mathcal{L}_{13}}\right)}. \quad (2.11)$$

If, as it often does, a single production mode dominates in a concrete model, Eq. (2.11) can be directly used to identify how large  $c_\gamma$  needs to be. In the case where several initial states contribute, a conservative lower bound is given by

$$|c_\gamma| > \sqrt{\frac{n_g}{n_\gamma} \frac{N}{\epsilon x_S^{13,g} \mathcal{L}_{13}}} = 2.7 \times \sqrt{\left(\frac{N}{20}\right) \left(\frac{5.8 \text{ fb}^{-1}}{\mathcal{L}_{13}}\right)}. \quad (2.12)$$

In Figs. 1 and 2, we plot the general relation between  $|c_\gamma|$  and  $|c_p|$  for the case of  $N = 20$  excess events, switching on one production channel at a time. The mass and total width are fixed at 750 and 45 GeV, respectively. The partial widths to diphotons,  $\Gamma_{\gamma\gamma}$ , and to the production mode,  $\Gamma_p$ , are assumed to be supplemented by decays to other possible final states,  $\Gamma_{\text{other}}$ , to make up the total width:

$$\Gamma_{\text{other}} \equiv \Gamma - \Gamma_{\gamma\gamma} - \Gamma_p. \quad (2.13)$$

Contours of fixed  $\text{BR}_{\text{other}} \equiv \Gamma_{\text{other}}/\Gamma$  are shown in dashed blue. From the left panels of the figures it is evident that for a given  $\text{BR}_{\text{other}}$  there exist two solutions, one with small and another with large  $c_\gamma$ . The shaded gray regions correspond to values of  $c_p$  and  $c_\gamma$ , for

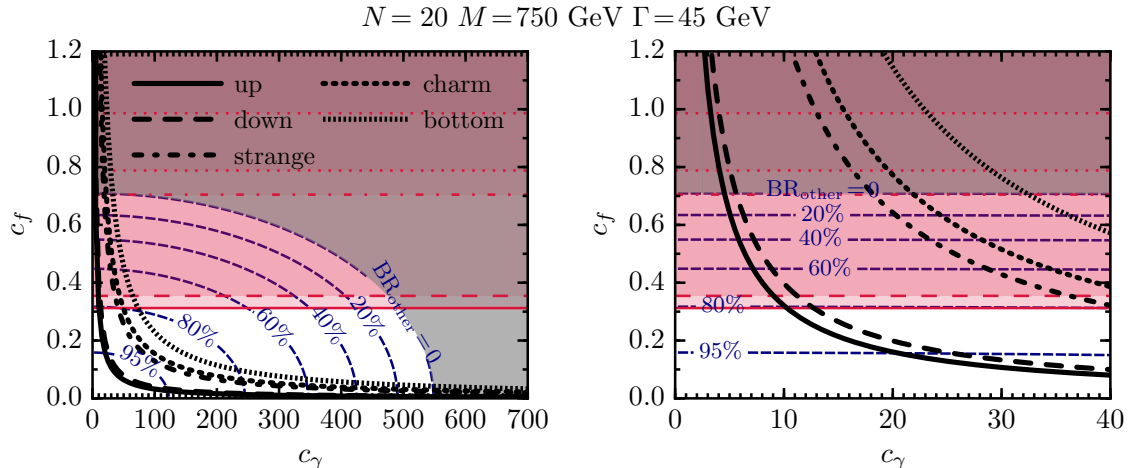


**Figure 2.** Black lines correspond to  $N = 20$  signal events in the diphoton analyses for  $M = 750 \text{ GeV}$  and  $\Gamma = 45 \text{ GeV}$ . Different dashed styles indicate the various production modes,  $u\bar{u}$ ,  $d\bar{d}$ ,  $s\bar{s}$ ,  $c\bar{c}$ , and  $b\bar{b}$ . Blue dashed lines are contours of fixed branching ratio to modes other than  $\gamma\gamma$  or the production mode. The red-shaded areas above the various horizontal lines, with dashed styles corresponding to the production modes, are excluded by dijet resonance searches due to decays to the production mode alone. The right panel is a blowup of the left one.

which the total width is larger than  $45 \text{ GeV}$ . Horizontal red lines and the corresponding shaded red regions indicate the parameter space excluded by  $8 \text{ TeV}$  dijet searches. We discuss them in the next section.

The lower bounds on  $c_\gamma$  in Eq. (2.11) are approximately the crossings of the black lines with the  $BR_{\text{other}} = 0$  contour at the lower  $c_\gamma$ . From Fig. 1 we see that either large  $c_g$  or large  $c_\gamma$  is necessary to accommodate the excess. From this point of view, since the production via quark fusion, Fig. 2, relies on  $c_f \lesssim 1$ , it may be considered a more natural possibility.

## 2.2 Interplay with previous LHC searches

Important additional information about the properties of the new particle can be obtained based on the non-observation of any of its decays in Run 1 of the LHC, in particular in the  $20 \text{ fb}^{-1}$  of data collected at  $\sqrt{s} = 8 \text{ TeV}$ .

We first consider limits from the diphoton resonance searches. The most relevant limit for the broad resonance hypothesis preferred by the ATLAS excess,  $\Gamma/M \approx 6\%$ , is the CMS limit

$$\sigma_8 \times BR_{\gamma\gamma} \lesssim 2.5 \text{ fb}, \quad (2.14)$$

which was derived for scalar resonances with  $\Gamma/M = 10\%$  [10]. For a narrow resonance, which might be preferred by the CMS data, the same search obtains the limit

$$\sigma_8 \times BR_{\gamma\gamma} \lesssim 1.3 \text{ fb}. \quad (2.15)$$

Somewhat weaker limits, of  $2.5$  and  $2.0 \text{ fb}$ , were obtained by ATLAS [11] and CMS [12], respectively, for RS gravitons with  $k = 0.1$ , which are also narrow.

decay mode $i \rightarrow$	$gg$	$q\bar{q}$	$t\bar{t}$	$WW$	$ZZ$	$hh$	$Zh$	$\tau\tau$	$Z\gamma$	$ee + \mu\mu$	
$(\sigma_8 \times \text{BR}_i)^{\text{max}}$ [fb]	4000 [13]	1800 [13]	500 [14]	60 [15]	60 [16]	50 [17]	17 [18]	12 [19]	8 [20]	2.4 [21]	
production $p =$	$gg$	2600	1200	320	38	38	32	11	7.7	5.1	1.5
$\left(\frac{\text{BR}_i}{\text{BR}_{\gamma\gamma}}\right)^{\text{max}}$	$u\bar{u}$	1500	690	190	23	23	19	6.5	4.6	3.1	0.9
	$d\bar{d}$	1600	700	200	23	23	20	6.7	4.7	3.1	0.9
	$s\bar{s}$	2300	1000	280	34	34	28	9.6	6.8	4.5	1.4
	$c\bar{c}$	2400	1100	300	36	36	30	10	7.3	4.8	1.5
	$b\bar{b}$	2700	1200	340	40	40	34	11	8.1	5.4	1.6

**Table 3.** Top: Bounds on 750 GeV resonances from 8 TeV LHC searches. Bottom: Derived bounds on ratios of branching fractions for different production channel assumptions. For  $gg$  production, bounds on the branching fraction to  $q\bar{q}$  are even tighter than indicated, since decays to  $gg$  will necessarily also be present and enter the dijet searches. The same applies to branching fraction to  $gg$  when the production is from quarks.

The compatibility of the observed excesses with the 8 TeV diphoton searches depends primarily on the parton luminosity ratio,  $r_p$ , listed in Tab. 2, since the selection efficiencies of the searches are similar. The ATLAS+CMS excess, Eq. (2.1), translates to

$$\sigma_8 \times \text{BR}_{\gamma\gamma} = \frac{\sigma_{13} \times \text{BR}_{\gamma\gamma}}{r_p} \approx \left(\frac{N}{20}\right) \times \{1.6, 2.6, 2.6, 1.8, 1.7, 1.5, 1.6, 1.6\} \text{ fb} \quad (2.16)$$

for the different production cases from Eq. (2.6). We see that  $N = 20$  excess events at 13 TeV are borderline compatible with the 8 TeV analyses, especially if the resonance is broad. The  $gg$  and heavy-quark production modes are somewhat favoured in this respect because their luminosities increase more rapidly with  $\sqrt{s}$ .

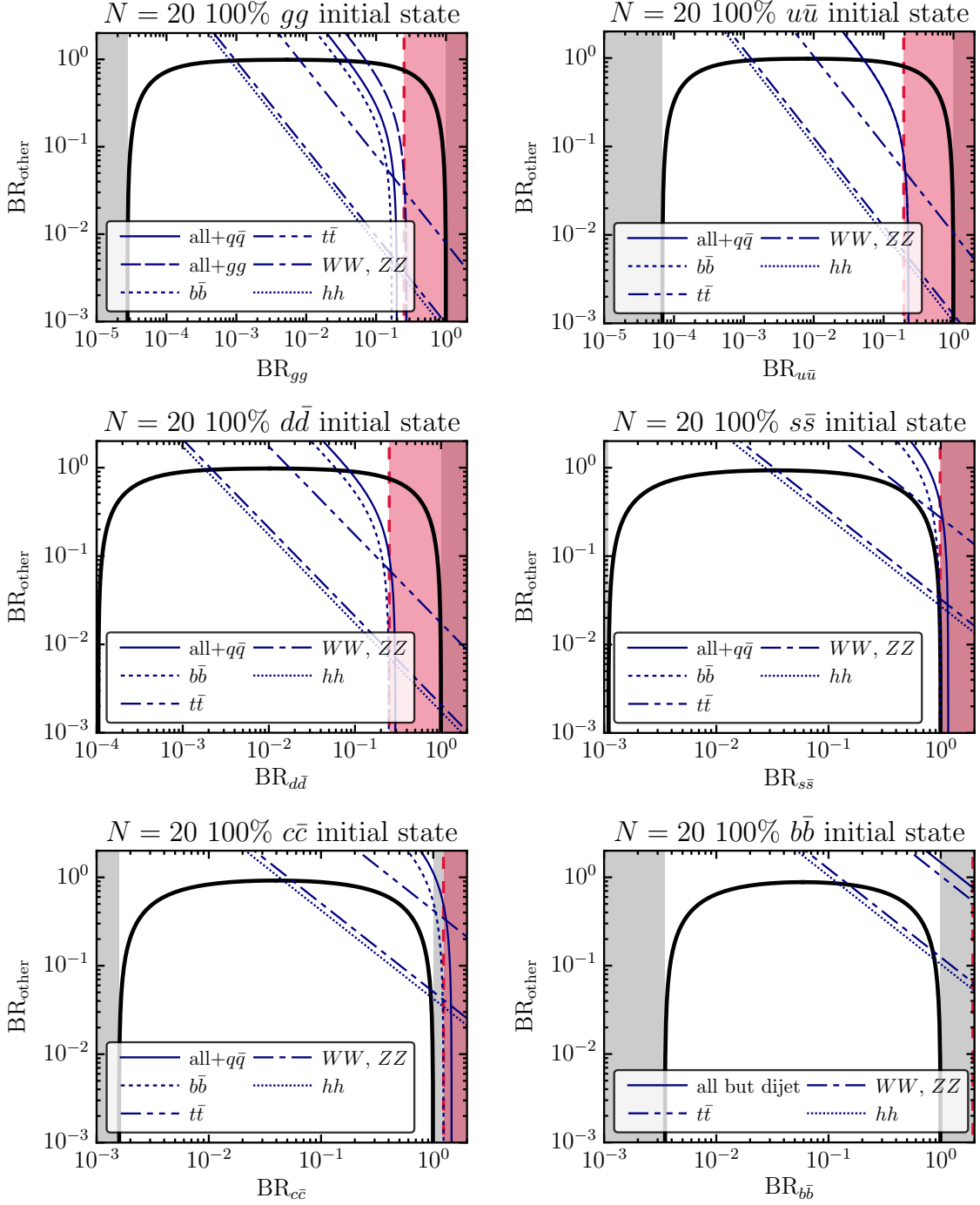
The ATLAS and CMS collaborations performed searches for resonant signals in many other final states as well. In Table 3 we list the various two-body final states relevant to a neutral color-singlet spin-0 particle, and the corresponding 95% C.L. exclusion limits,  $(\sigma_8 \times \text{BR}_i)^{\text{max}}$ , from the 8 TeV searches. Searches for dijet resonances that employ  $b$  tagging, and would have enhanced sensitivity to  $b\bar{b}$  final states, only address resonances heavier than 1 TeV [22, 23], but the limits from  $q\bar{q}$  searches still apply to  $b\bar{b}$ . The recent 13 TeV dijet searches [24, 25] do not cover the mass range around 750 GeV at all, due to triggering limitations. We also note that the limits quoted in Table 3 are approximate. In general, they do have some dependence on the width of the resonance, its spin, etc.

Table 3 also lists the resulting constraints on the ratios of branching fractions of the particle, for different production channel assumptions. They are computed as

$$\left(\frac{\text{BR}_i}{\text{BR}_{\gamma\gamma}}\right)^{\text{max}} = r_p \frac{(\sigma_8 \times \text{BR}_i)^{\text{max}}}{\sigma_{13} \times \text{BR}_{\gamma\gamma}}, \quad (2.17)$$

where we use Eq. (2.1) and the parton luminosity ratios  $r_p$  from Table 2.

There is always a constraint from decays to dijets since we take the resonance to couple to either  $gg$  or  $q\bar{q}$  for production. Also, the production cross section needs to be relatively



**Figure 3.** The required branching fraction into modes other than the production mode and  $\gamma\gamma$ ,  $BR_{\text{other}}$ , as a function of the production mode branching fraction, for  $N = 20$  and  $\Gamma = 45 \text{ GeV}$ . Different plots correspond to different production mechanisms. The edges of the gray regions indicate the minimal and maximal branching ratio to the production mode. Red regions are excluded by 8 TeV dijet resonance searches. Thin lines described in the legend show the maximal branching fractions allowed by 8 TeV searches into final states from Tab. 3. The label “all” includes all the final states from the table except for  $gg$  and  $q\bar{q}$ .

large to accommodate the excess without too large  $c_\gamma$ , so limits on dijet resonances may restrict part of the parameter space of a concrete realisation. For the case in which a single production channel dominates, we obtain upper limits on  $c_p$  by saturating the  $gg$  or  $q\bar{q}$  dijet bounds:

$$\begin{aligned} \text{BR}_p &< \sqrt{n_p \frac{M (\sigma_8 \times \text{BR}_p)^{\text{excl}}}{\Gamma x_S^{8,p}}} \approx \{25, 19, 25, 99, 124, 193\}\% \times \left(\frac{45 \text{ GeV}}{\Gamma}\right)^{1/2}, \\ |c_p| &< \{97, 0.31, 0.35, 0.70, 0.79, 0.99\} \times \left(\frac{\Gamma}{45 \text{ GeV}}\right)^{1/4}. \end{aligned} \quad (2.18)$$

The corresponding excluded regions in the  $c_p$ - $c_\gamma$  planes of Figs. 1 and 2 are the red-shaded areas.

By combining Eq. (2.18) with Eqs. (2.4) and (2.9), we obtain a second lower bound on  $\text{BR}_{\gamma\gamma}$  and  $c_\gamma$ ,

$$\begin{aligned} \text{BR}_{\gamma\gamma} &> \{1.0, 2.9, 3.6, 9.7, 11, 16\} \times 10^{-4} \times \left(\frac{N}{20}\right) \left(\frac{5.8 \text{ fb}^{-1}}{\mathcal{L}_{13}}\right) \left(\frac{45 \text{ GeV}}{\Gamma}\right)^{1/2}, \\ |c_\gamma| &> \{5.5, 9.4, 11, 17, 19, 22\} \times \sqrt{\left(\frac{N}{20}\right) \left(\frac{5.8 \text{ fb}^{-1}}{\mathcal{L}_{13}}\right) \left(\frac{\Gamma}{45 \text{ GeV}}\right)^{1/4}}. \end{aligned} \quad (2.19)$$

Depending on the width and the production mechanism, these bounds can be stronger or weaker than those in Eqs. (2.8) and (2.11).

Figure 3 shows the required branching fraction  $\text{BR}_{\text{other}}$  to modes other than the production mode and  $\gamma\gamma$  as a function of the branching fraction of the production mode,  $\text{BR}_p$ . The black lines correspond to  $N = 20$  signal events in the 13 TeV diphoton analyses. These plots highlight the importance of  $\text{BR}_{\text{other}}$ , which in most of the viable parameter space is the dominant branching fraction. In blue lines, it is also shown to which extent  $\text{BR}_{\text{other}}$  can be attributed to various decays into Standard Model particles, in view of the 8 TeV LHC bounds on such decays. We see that when the diphoton signal is achieved by a large coupling to gluons/quarks and a small coupling to photons (right-hand side of the plots), it may be difficult to obtain  $\Gamma = 45 \text{ GeV}$  with decays to SM particles alone (if we neglect the possibility of large branching fractions to  $\nu\bar{\nu}$  or multibody final states). On the other hand, in the case of a small coupling to gluons/quarks and a large coupling to photons (left side of the plots) there is no such limitation.

### 3 Models

We now turn to discuss concrete models. First, in section 3.1, we discuss interpretations of the resonance as a scalar that is a singlet under the SM gauge group. Next, in section 3.2, we interpret it as a doublet of  $SU(2)_L$ . Finally, in section 3.3 we analyse the resonance being a heavy Higgs of the MSSM.

### 3.1 SM-singlet scalar

The most general Lagrangian for a singlet scalar coupled to the SM, up to dimension-5 terms, is

$$\begin{aligned} \mathcal{L}_{\text{singlet}} = & (\mu\Phi + \kappa_{H1}\Phi^2)H^\dagger H \\ & + \frac{\Phi}{f} \left( \kappa_g \frac{\alpha_s}{8\pi} G_{\mu\nu} G^{\mu\nu} + \kappa_Y \frac{\alpha_1}{8\pi} B_{\mu\nu} B^{\mu\nu} + \kappa_W \frac{\alpha_2}{8\pi} W_{\mu\nu} W^{\mu\nu} + \kappa_{H2} |D_\mu H|^2 + \kappa_{H3} |H|^4 \right) \\ & - \frac{\Phi}{f} \left( Y_{ij}^d H \bar{Q}_i d_j + Y_{ij}^u \tilde{H} \bar{Q}_i u_j + Y_{ij}^e H \bar{L}_i e_j + h.c. \right). \end{aligned} \quad (3.1)$$

We will first discuss the renormalizable model in which only the terms on the first line are present. We will then consider a model where the diphoton and digluon couplings of the second line are generated by additional vectorlike fermions. Finally, we will consider the dilaton model of Ref. [26] in which the coefficients  $\kappa_{g,Y,W}$  are related to the  $\beta$  functions in the low-energy effective theory.

#### 3.1.1 Renormalizable model

We consider the case with only the renormalizable couplings in Eq. (3.1). The  $\kappa_{H1}$  term induces mixing of  $\Phi$  with the SM CP-even doublet component of  $H$ , and we obtain two mass eigenstates,  $\mathcal{S}$  and the observed 125 GeV Higgs  $h$ . This results in  $\mathcal{S}$  having tree-level couplings proportional to those of the SM Higgs but suppressed by a universal factor,

$$g_i^{\mathcal{S}} = s_\alpha g_i^{h_{\text{SM}}}, \quad (3.2)$$

where  $s_\alpha \equiv \sin \alpha$ ,  $\alpha$  being the mixing angle. This mixing also modifies the couplings of the observed 125 GeV Higgs boson with respect to what they would be in the SM. The modified couplings scale as  $\cos \alpha$  with respect to their SM values. We must thus have  $s_\alpha \lesssim 0.2$  to ensure that these modifications are compatible with Higgs and particularly electroweak precision measurements [27]. The coupling to the light quarks is thus negligible, therefore the production must be gluonic. At one-loop level, SM particles generate an effective  $c_g$  and  $c_\gamma$ . To get the largest possible  $c_g$  and  $c_\gamma$  we take  $s_\alpha = 0.2$  and obtain using the expressions for the top and  $W$ -loop contributions in Ref. [28],

$$c_g = 1.6, \quad c_\gamma = 0.09. \quad (3.3)$$

If we assume a 45 GeV width, we need  $|c_g c_\gamma| \approx 530$  to accommodate the excess, so these numbers are far too small. Even if we allow for a smaller width we still cannot satisfy the bound in Eq. (2.11).

Clearly we need large contributions from BSM states to either  $c_{\gamma,g}$  or to the irrelevant couplings of  $\Phi$  to light quarks in Eq. (3.1) to explain the size of the excess. We will next explore BSM contributions that can boost  $c_g$  and  $c_\gamma$  with respect to this renormalizable case with no additional states.

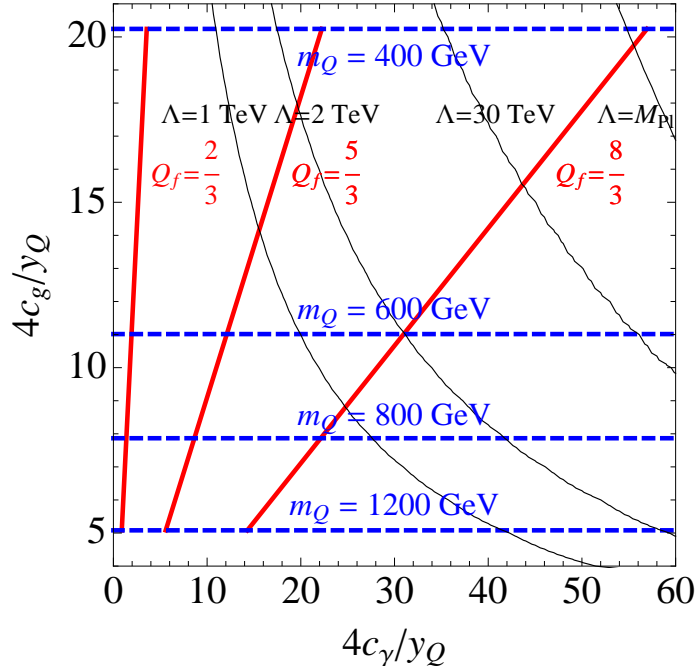


**Figure 4.** Contributions of vectorlike fermions with charge  $Q_f$  and Yukawa coupling  $y_Q$  to the photonic,  $c_\gamma$ , and gluonic,  $c_g$ , couplings of a SM singlet  $\mathcal{S}$ , scaled by  $4/y_Q$ . All points in the plot produce  $N = 20$  excess events. Also shown are contours of the scale  $\Lambda$  at which the coupling  $y_Q$  becomes strong ( $\mathcal{O}(4\pi/\sqrt{N_c})$ ), assuming we take it to be just large enough at each point in the  $c_g$ - $c_\gamma$  plane to obtain  $|c_g c_\gamma| = 530$  and explain the excess.

### 3.1.2 Boosting $c_\gamma$ , $c_g$ with new vectorlike fermions

To investigate whether new colored and charged particles can generate large enough  $c_{g,\gamma}$ , we consider the minimal case of an additional vectorlike fermion, a triplet under QCD with electric charge  $Q_f$ , that couples to  $\Phi$  as

$$\mathcal{L} = -y_Q \Phi \bar{Q} Q - m_Q \bar{Q} Q. \quad (3.4)$$

The fermion loop generates  $c_{g,\gamma}$ . Any mixing of  $\Phi$  with the Higgs doublet would dilute the vectorlike loop contributions to the diphoton and digluon couplings (that would be generally larger than the SM loop contributions) of the mass eigenstate  $\mathcal{S}$ . Thus, we assume that the mixing, which is in any case constrained to be small, to be negligible and the mass eigenstate to be  $\mathcal{S} = \Phi$ .

We first consider the case in which we assume the resonance is broad with a 45 GeV width. The fermion  $Q$  contributes

$$c_g = g_s^2 y_Q \tilde{A}_{1/2}(\tau_Q), \quad (3.5)$$

$$c_\gamma = 2N_c Q_f^2 e^2 y_Q \tilde{A}_{1/2}(\tau_Q), \quad (3.6)$$

where  $\tau_Q = M^2/(4m_Q^2)$  and

$$\tilde{A}_{1/2}(\tau) = 2\tau^{1/2} A_{1/2}(\tau) = 4\tau^{-3/2} [\tau + (\tau - 1)f(\tau)], \quad (3.7)$$

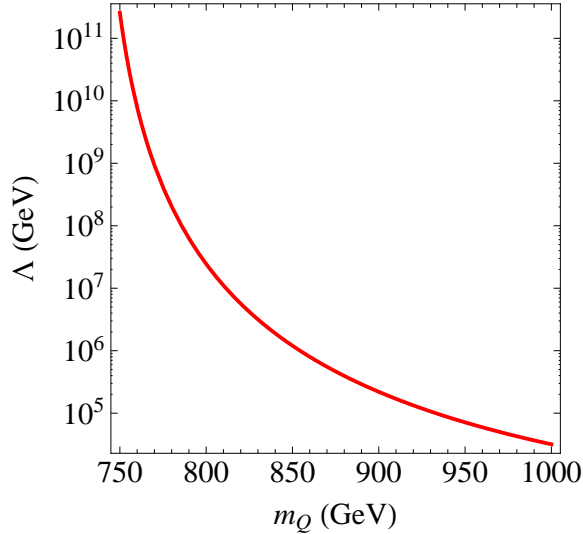


**Figure 5.** For a narrow-width singlet scalar, the scale of breakdown of perturbativity as a function of the charge-4/3 vectorlike fermion mass  $m_Q$ , assuming we take the required  $y_Q$  to explain the excess. For  $m_Q \lesssim 750$  GeV the  $\beta$  function is negative, so the theory is perturbative in this region. The coupling  $y_Q$  varies from 2.4 to 3.3 for the range of  $m_Q$  shown.

with  $f(\tau)$  defined in Ref. [28]. For  $m_Q < M/2$  we obtain the constraint  $y_Q \lesssim 0.7$  by requiring  $\Gamma(\mathcal{S} \rightarrow Q\bar{Q}) < 45$  GeV. This would lead to very small values of  $c_{g,\gamma}$  and we thus take  $m_Q > M/2$ . In Fig. 4, we show the values of  $c_{g,\gamma}$  generated as  $m_Q$  is varied between 400 GeV and 1.2 TeV. The values of  $c_{g,\gamma}$  for  $y_Q = 4$  can be directly read off from Fig. 4 and one can easily find them for other  $y_Q$  values by keeping in mind that  $c_{g,\gamma}$  scale linearly with  $y_Q$ .

We see that unless  $y_Q$  is large we cannot obtain  $|c_g c_\gamma| \approx 530$  required to explain the excess. In some regions of the parameter space, this implies a low cut-off for the theory at the scale in which  $y_Q$  becomes strongly coupled. In Fig. 4 we also show contours of the scale  $\Lambda$  at which the coupling  $y_Q$  becomes strong ( $\mathcal{O}(4\pi/\sqrt{N_c})$ ), assuming we take it to be just large enough at each point in Fig. 4 to explain the excess. We also mark the region (below the red dotted curve) where the UV contribution from the cut-off (evaluated by assuming a fermion of same charge but with mass at the cut-off and  $y_Q = 4\pi/\sqrt{N_c}$ ) is as large as the contribution from  $Q$ . It is clear that the theory becomes strongly coupled below 2 TeV unless we take a large value for the electric charge, e.g.  $Q_f = 8/3$ . For a large charge, the negative contribution to the running proportional to  $y_Q g'^2$  can actually push the cut-off to values as high as 100 TeV, as one can see from the top right of Fig. 4. Note that we cannot push the strong coupling scale higher by taking a large number,  $N_f$ , of flavors or larger QCD representations and thus achieve a smaller  $y_Q$ , as there are terms proportional to  $N_f y_Q^2$  and  $N_c y_Q^2$  that appear in the RGE for  $y_Q$ .

We note that the partial width to photons or gluons never exceeds 5 GeV so we need a large width to particles other than photons or gluons to explain the 45 GeV width we have assumed here. The dijet constraint  $c_g \lesssim 97$  (see Eq. (2.18)) is satisfied in the full

parameter space even after rescaling  $y_Q$  appropriately to explain the signal, assuming that there are no dijet final states other than  $gg$ .

We now consider the case in which the resonance is narrow and there are no decays except to  $gg$  and  $\gamma\gamma$ . In this case, the total width is dominated by  $\Gamma(\mathcal{S} \rightarrow gg)$  as  $\Gamma(\mathcal{S} \rightarrow gg) \gg \Gamma(\mathcal{S} \rightarrow \gamma\gamma)$  for  $\mathcal{O}(1)$  charges (see Eq. (3.6)). We then only need a  $c_\gamma \sim 2.7$  in accordance with Eq. (2.11). In Fig. 5 we show the scale of breakdown of perturbativity assuming the required  $y_Q$  to obtain  $c_\gamma \sim 2.7$ , as a function of  $m_Q$  from the loop of a vectorlike fermion with  $Q_f = 4/3$ . We see that the theory is perturbative up to high scales even though we took only  $Q_f = 4/3$ .

We thus find that for a  $\Gamma \approx 45$  GeV singlet resonance the size of the excess suggests strongly coupled physics at a few TeV unless there are fermions around or below the mass of the resonance with large electric charge. For the narrow width case we still need to require additional charged states but the theory can be perturbative. The hints of strongly coupled physics motivate us to examine in more detail a popular strongly coupled scalar candidate, the dilaton.

### 3.1.3 The dilaton

We consider the model of Ref. [26] in which the couplings of the dilaton in the electroweak broken phase are given by

$$\mathcal{L}^{\text{dil}} = \frac{\Phi}{f} \left( \sum_f m_f \bar{f} f + 2 \left( m_W^2 W^+ W^- + \frac{m_Z^2}{2} Z^2 \right) + \frac{\kappa_g \alpha_s}{8\pi} G_{\mu\nu} G^{\mu\nu} + \frac{\kappa_\gamma \alpha_{EM}}{8\pi} F_{\mu\nu} F^{\mu\nu} \right). \quad (3.8)$$

Furthermore, in general, there will be a mixing term with the SM Higgs, that can arise from either the potential term  $\Phi H^\dagger H$  or from kinetic mixing [29], so that finally we obtain two mass eigenstates,  $\mathcal{S}$  and the observed 125 GeV Higgs  $h$ , where

$$\mathcal{S} = s_\alpha h_{\text{SM}} + c_\alpha \Phi, \quad (3.9)$$

and we expect  $s_\alpha = \mathcal{O}(v/f)$ . We thus have for the coupling to fermions and gauge bosons

$$g_{V,f}^{\mathcal{S}} = \xi g_{V,f}^{h_{\text{SM}}}, \quad \text{with } \xi = s_\alpha + \frac{v}{f} c_\alpha. \quad (3.10)$$

For the dilaton, the couplings  $\kappa_{g,\gamma}$  are completely determined using the low-energy theorems and scale invariance [26]. We obtain for the dilaton coupling to gluons

$$\frac{\Phi}{f} \frac{\sum_{\text{heavy}} b_0^i \alpha_s}{8\pi} G_{\mu\nu} G^{\mu\nu}, \quad (3.11)$$

where  $b_0^i$  is the contribution of the field  $i$  to the QCD  $\beta$  function,

$$\beta_i = \frac{b_0^i g_s^3}{16\pi^2}, \quad (3.12)$$

and the sum is over all particles heavier than the scale  $f$ . Scale invariance implies

$$\sum_{\text{heavy}} b_0^i + \sum_{\text{light}} b_0^i = 0, \quad (3.13)$$

so that we finally obtain

$$\kappa_g^\Phi = - \sum_{\text{light}} b_0^i. \quad (3.14)$$

If the dilaton is heavier than the top quark (like here) and the full SM is part of the conformal sector, we must sum over all coloured SM states, which gives  $\sum_{\text{light}} b_0^i = -7$ . Note that if we do not include all SM fields in the conformal/composite sector [30] but keep some SM fields elementary  $\sum_{\text{light}} b_0^i$  would change. Similarly one obtains [26]

$$\kappa_\gamma = -11/3. \quad (3.15)$$

We will require  $f \gtrsim M$ , which gives for the total width,

$$\Gamma \lesssim 25 \text{ GeV} \quad (3.16)$$

The maximal number of events is generated for the maximal allowed width. This is because the narrow width would require a larger  $f$  which would decrease the production but keep the branching ratio to photons unchanged. Thus taking  $f = M$  we find

$$c_g = 21, \quad c_\gamma = 0.7, \quad (3.17)$$

where we have again assumed  $s_\alpha = \mathcal{O}(v/f)$ . We find that VBF production is negligible so that the dominant mode is gluon initiated. For  $\Gamma = 25 \text{ GeV}$  we need from Eq. (2.9)  $|c_g c_\gamma| \sim 395$  to explain the excess, which is much larger than the product we get from the numbers above in Eq. (3.17). Thus, we need additional large contributions to the QCD and QED  $\beta$  functions below the scale  $f$ ,

$$\begin{aligned} \Delta c_g &= \frac{2g_s^2 \Delta b_{\text{QCD}} M}{f}, \\ \Delta c_\gamma &= \frac{2e^2 \Delta b_{\text{QED}} M}{f}. \end{aligned} \quad (3.18)$$

For  $n_f$  additional vectorlike colour-triplet,  $SU(2)_L$ -singlet fermions we have

$$\begin{aligned} \Delta b_{\text{QED}} &= \frac{4N_c n_f}{3} Q_f^2, \\ \Delta b_{\text{QCD}} &= \frac{2}{3} n_f, \end{aligned} \quad (3.19)$$

where  $Q_f$  is the electric charge of the fermion. Clearly to enhance  $c_g$  or  $c_\gamma$  to a magnitude such that  $|c_g c_\gamma| \approx 530$  as required by the data to explain the excess, we need either an unusually large charge  $Q_f$  or a very large number of flavours  $n_f$  of additional fermions below the TeV scale. This scenario thus does not seem feasible.

Still, even if it is possible to boost  $c_g$  or  $c_\gamma$  in some variant of the above setup, dilaton models would in general be strongly constrained by 8 TeV diboson searches. From Table 3 these constraints are

$$\frac{\text{BR}(\mathcal{S} \rightarrow WW/ZZ)}{\text{BR}(\mathcal{S} \rightarrow \gamma\gamma)} \lesssim 38, \quad (3.20)$$

whereas we obtain this ratio to be  $\mathcal{O}(10^4)$  if we use the numbers in Eq. (3.17).

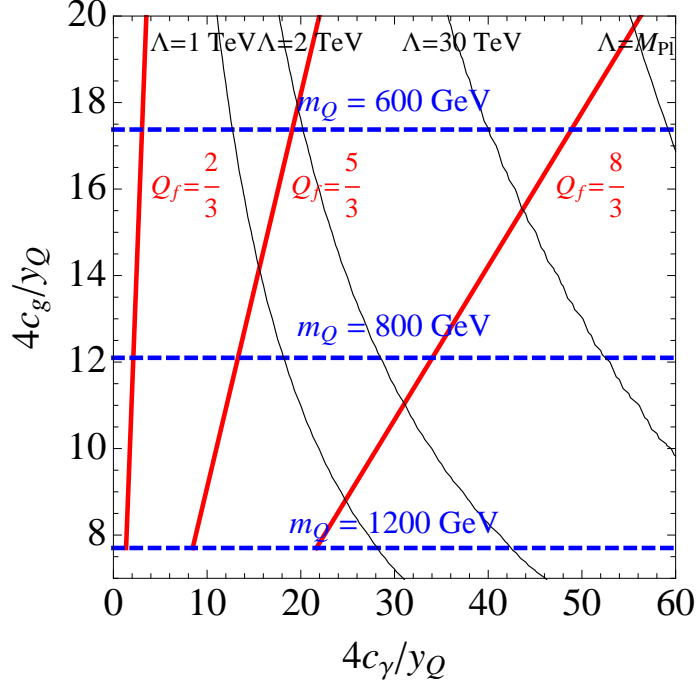


**Figure 6.** Contributions of vectorlike fermions with charge  $Q_f$  and Yukawa coupling  $y_Q$  to the photonic,  $c_\gamma$ , and gluonic,  $c_g$ , couplings of a pseudoscalar SM singlet  $\mathcal{S}$ , scaled by  $4/y_Q$ . In grey are contours of the scale  $\Lambda$  at which the coupling  $y_Q$  becomes strong ( $\mathcal{O}(4\pi/\sqrt{N_c})$ ), where we have fixed  $y_Q(M)$  by requiring the correct signal size.

### 3.1.4 A pseudoscalar

We now consider the case of a pseudoscalar. It can appear in composite models as a pseudo-Nambu-Goldstone boson (PNGB) [31]. Unlike the scalar it cannot mix with the SM Higgs and some couplings like those to longitudinal  $W$ 's and  $Z$ 's in Eq. (3.1) are not allowed. This is therefore an example, where unlike for the dilaton, the ratio of the partial widths to electroweak bosons and photons is not expected to be very large and it is thus not so severely constrained by diboson searches. The most general Lagrangian terms are

$$\begin{aligned}
\mathcal{L} = & -\frac{1}{16\pi^2} \frac{1}{4} \frac{c_B}{M} \mathcal{S} B^{\mu\nu} \tilde{B}_{\mu\nu} - \frac{1}{16\pi^2} \frac{1}{4} \frac{c_W}{M} \mathcal{S} W^{a\mu\nu} \tilde{W}_{\mu\nu}^a - \frac{1}{16\pi^2} \frac{1}{4} \frac{c_g}{M} \mathcal{S} G^{\mu\nu,a} \tilde{G}_{\mu\nu}^a \\
& - \frac{\mathcal{S}}{f} \left( Y_{ij}^d H \bar{Q}_i \gamma^5 d_j + Y_{ij}^u \tilde{H} \bar{Q}_i \gamma^5 u_j + Y_{ij}^e H \bar{L}_i \gamma^5 e_j + h.c. \right) \\
\supset & -\frac{1}{16\pi^2} \frac{1}{4} \frac{c_\gamma}{M} \mathcal{S} F^{\mu\nu} \tilde{F}_{\mu\nu} - \frac{1}{16\pi^2} \frac{1}{4} \frac{c_g}{M} \mathcal{S} G^{\mu\nu,a} \tilde{G}_{\mu\nu}^a + y_Q \mathcal{S} \bar{Q} \gamma^5 Q, \tag{3.21}
\end{aligned}$$

where  $f$  is a SM fermion and we have also included a coupling to a vectorlike quark  $Q$ . Assuming a 45 GeV total width and following the same procedure as in Sec. 3.1.2, we show in Fig. 6 the contribution of the vectorlike quark loop to  $c_g$  and  $c_\gamma$  and the scale where  $y_Q$  becomes non-perturbative. We find again that, only for vectorlike fermions with large electric charges, the theory can be perturbative up to high scales. If we allow for a smaller width and include only  $gg$  and  $\gamma\gamma$  decays, the total width will be dominated by

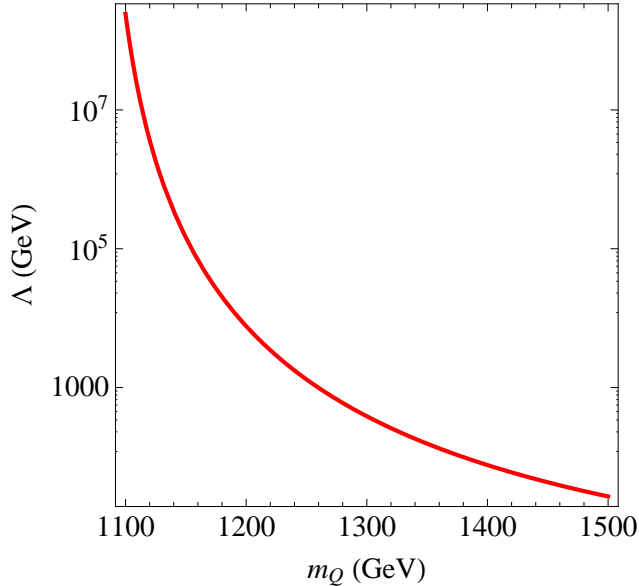


**Figure 7.** For a narrow-width singlet pseudoscalar, the scale of breakdown of perturbativity as a function of the charge-4/3 vectorlike fermion mass  $m_Q$ , assuming we take the required  $y_Q$  to explain the excess. For  $m_Q \lesssim 1100$  GeV the  $\beta$  function is negative, so the theory is perturbative in this region. The coupling  $y_Q$  varies from 2.4 to 3.4 for the range of  $m_Q$  shown.

$\Gamma(\mathcal{S} \rightarrow gg)$  as  $\Gamma(\mathcal{S} \rightarrow gg) \gg \Gamma(\mathcal{S} \rightarrow \gamma\gamma)$  and from Eq. (2.11) we would only need  $c_\gamma \sim 2.7$ . In Fig. 7 we show, as a function of  $m_Q$ , the scale of breakdown of perturbativity by fixing  $y_Q$  appropriately to obtain  $c_\gamma \sim 2.7$  from a vectorlike fermion with  $Q_f = 4/3$ . We find, as in the scalar case, that the theory is perturbative up to high scales with even smaller charges than in the case of the 45 GeV width.

### 3.2 Excluding the general pure 2HDM

In this part we discuss the possibility of explaining the excess within the framework of the general two-Higgs-doublet model (2HDM), assuming no additional states beyond the additional doublet. It is useful to describe the theory in the so-called Higgs basis [32], where only one of the two doublets, which corresponds to the SM Higgs, acquires a VEV. The SM-like Higgs doublet,  $H_a$ , has a VEV equal to 246 GeV and a CP-even component with exactly SM-like couplings, whereas the other doublet,  $H_b$ , which contains the charged and pseudoscalar mass eigenstates, has a vanishing VEV.

The coupling

$$\lambda_V(H_b^\dagger H_a)(H_a^\dagger H_a) + h.c. \quad (3.22)$$

causes a misalignment between the Higgs basis and the CP-even mass basis that is of order  $\lambda_V v/M$  [33]. If  $\lambda_V \lesssim \mathcal{O}(1)$  we are in the so-called decoupling limit and can think of the ratio  $\epsilon \equiv \lambda_V v/M$  as our formal expansion parameter (see Ref. [34] and references therein for relevant discussions). The above coupling induces a coupling of the CP even part,  $H^0$ , and the pseudoscalar,  $A^0$ , to the electroweak gauge bosons,  $VV$ . At the same time, it

causes a deviation from SM values in the  $h^0VV$  coupling,  $h^0$  being the lighter CP-even state. The value of  $\lambda_V$  is thus constrained by electroweak precision measurements. Using the expressions in Ref. [32] we find the constraint

$$\lambda_V < 3, \quad (3.23)$$

which shows that we are in fact in the decoupling limit as  $\epsilon < 0.3$ .

One interesting consequence of the fact that  $v^2/M^2 \ll 1$ , is that the splitting in the mass square between the neutral CP-even state,  $H^0$ , and the odd one,  $A$ , which is due to the coupling

$$\lambda_5(H_a^\dagger H_b)^2 + h.c., \quad (3.24)$$

is of the order of  $\lambda_5 v^2/M^2$  and thus generically small,

$$\delta m = |m_{H^0} - m_{A^0}| \lesssim \frac{v^2}{M^2} \times \frac{M}{2} = 42 \text{ GeV} \quad (3.25)$$

for an  $\mathcal{O}(1)$  value of  $\lambda_5$ . As  $\delta m$  is compatible with the width of the excess, it is quite possible that actually the observed signal arises due to the presence of these two neighbouring states.

We now show that the general pure 2HDM cannot account for the observed excess. We note that in the Higgs basis the couplings of the heavy states to the light quarks can differ from those of the SM Higgs, as was exploited in Ref. [35]; this is because  $H_b$  acquires no VEV and thus its couplings to SM fermions does not contribute to their masses. In particular, the couplings of  $H_b$  to the light quarks may be compatible with the ones extracted in the model-independent discussion (see Fig. 2). Thus, in this part we consider production through either quark-antiquark or gluon fusion. In addition, as the signal can be generically accounted for by the presence of both  $H^0$  and  $A^0$ , we should consider the production and decay of each of these. We emphasise that to be conservative we do not require the width to be equal to 45 GeV as the excess could be explained by the two narrower states separated in mass by few tens of GeVs, which would be consistent with the reported diphoton spectrum. We denote by  $N_H$  and  $N_A$  the number of events from the production and decay of  $H^0$  and  $A^0$ , respectively. In the CP limit we can assume no interference between the two different production modes.

**Gluon-gluon production** Assuming that the masses of  $A^0$  and  $H^0$  are less than 45 GeV apart, both states would contribute to the excess. For the total width of the resonance to not exceed 45 GeV it is necessary that

$$Y^2 = \sum_f \beta_f y_f^2 < 0.5, \quad (3.26)$$

where  $y_f$  is the coupling of  $H^0$  and  $A^0$  to the SM fermions,

$$y_f \bar{Q}_L (H^0 + iA^0) f_R + h.c. \quad (3.27)$$

and

$$\beta_f = \sqrt{1 - \frac{4m_f^2}{M^2}}, \quad (3.28)$$

with  $m_f$  being the fermion mass. Note that for the same coupling,  $y_f$ , the fermionic loop contribution decreases with the mass of the fermion. Thus, we find that for a fixed partial width to fermions (and thus a fixed  $Y^2$ ), to maximise the fermionic loop contributions, we need to take  $y_t/y_{f'} \gg 1$ , where  $y_t$  is the coupling to the top and  $y_{f'}$  the coupling to fermions other than the top. It is possible to bound the contributions from  $A^0$  because, unlike  $H^0$ , in the CP limit, its couplings to the photons and gluons are only due to fermion loops. The total number of events from pseudoscalar decays can be derived from Eq. (2.4),

$$N_A = 8.0 \times 10^5 \times \text{BR}_{\gamma\gamma} \times \frac{\Gamma(A^0 \rightarrow gg)}{\Gamma(A^0)} \times \frac{\Gamma(A^0)}{45 \text{ GeV}} < 8.0 \times 10^5 \times \frac{\Gamma(A^0 \rightarrow gg) \times \Gamma(A^0 \rightarrow \gamma\gamma)}{\Gamma(A^0 \rightarrow f\bar{f})^2}, \quad (3.29)$$

where

$$\begin{aligned} \Gamma(A^0 \rightarrow gg) &= \frac{y_t^2 \alpha_s^2 m_{A^0}^3}{32\pi^3 m_t^2} \left| \sum_f A_f^{A^0} \right|^2, \\ \Gamma(A^0 \rightarrow \gamma\gamma) &= \frac{y_t^2 \alpha^2 m_{A^0}^3}{64\pi^3 m_t^2} \left| \sum_f N_c Q_f^2 A_f^{A^0} \right|^2, \end{aligned} \quad (3.30)$$

with  $A_f^{A^0}$  a loop function of a single Dirac fermion, see for example [28]. As explained above, taking  $y_t \gg y_{f'}$  one can now evaluate the upper bound in Eq. (3.29),

$$N_A < 0.02, \quad (3.31)$$

where we have used  $\Gamma(A^0 \rightarrow t\bar{t}) = 0.11 M y_t^2$  from Table 1. We thus conclude that the pseudoscalar contributions are negligibly small in this case.

Next we consider the contribution from  $H^0$  production. To explain the signal we require that all 20 signal events must be from  $H^0$  decays,

$$20 = N_H < 2.0 \times 10^4 (\text{GeV}^{-1}) \times \frac{\Gamma(H^0 \rightarrow gg)}{\Gamma(H^0 \rightarrow t\bar{t})} \times \Gamma(H^0 \rightarrow \gamma\gamma). \quad (3.32)$$

Now, as above, we use  $y_t \gg y_{f'}$  to maximise the ratio  $\Gamma(H^0 \rightarrow gg)/\Gamma(H^0 \rightarrow t\bar{t})$  which then becomes independent of  $y_t$ . Using Table 1, we substitute  $\Gamma(H^0 \rightarrow \gamma\gamma) = 1.99 \times 10^{-7} M c_\gamma^2$  to obtain

$$c_\gamma > 66. \quad (3.33)$$

The real scalar contributions arise both due to fermionic loops and loops including the charged electroweak vector bosons and heavy Higgs bosons. We note that the contributions related to the heavy charged Higgs affect the total width of  $H^0$  only at subleading order due to its large mass. In order to check whether the general 2HDM can account for such a value of  $c_\gamma$  we have added up the loop contributions from the top quark, the  $W$  and the charged Higgs (see e.g. [28]) allowing for maximal constructive interference. In the Higgs basis the two couplings that can parametrize these contributions are  $\lambda_V$ , defined in Eq. (3.23), and

$$\lambda_{H^+}(H_a^\dagger H_b)(H_b^\dagger H_a) + h.c. \quad (3.34)$$

where the term proportional to  $\lambda_{H^+}$  ( $\lambda_V$ ) generates the charged-Higgs ( $W$ ) loop-induced contributions. We take the maximal value (already mentioned above)  $\lambda_V < 3$  allowed by electroweak precision constraints. The contributions to  $c_\gamma$  proportional to  $\lambda_{H^+}$  are unconstrained and can be significantly larger. However, we find that even if we take  $\lambda_{H^+} = 16\pi^2$  we can only obtain  $c_\gamma$  as large as 5. If we take  $\lambda_{H^+}$  to its perturbative limit  $16\pi^2/\sqrt{3}$  (such that loop contributions are at least a third of tree-level ones) we find  $c_\gamma < 3$ . Therefore, we conclude that production due to gluon fusion processes cannot account for the observed anomaly.

**Quark-antiquark production** As argued above, in general the heavy states can have sizable couplings to the first two generations. Ignoring possible severe constraints from flavour physics we find that the weakest bound is from production due to  $u\bar{u}$ . Again we bound the pseudoscalar contribution first. Using Eq. (2.4) we have

$$N_A = 8.0 \times 10^3 \times \text{BR}_{\gamma\gamma} \times \frac{\Gamma(A^0 \rightarrow u\bar{u})}{\Gamma(A^0)} \frac{\Gamma(A^0)}{\text{GeV}} = 8.0 \times 10^3 \times \frac{\Gamma(A^0 \rightarrow u\bar{u})}{\Gamma(A^0)} \frac{\Gamma(A^0 \rightarrow \gamma\gamma)}{\text{GeV}}. \quad (3.35)$$

As the up-quark loop contributes negligibly to  $\Gamma(A^0 \rightarrow \gamma\gamma)$  compared to the top-quark loop, the above expression is proportional to  $y_u^2 y_t^2 / Y^2$  where all the other fermionic couplings are zero. Keeping the bound from Eq. (3.26) in mind, this is maximised for  $y_u^2 = 0.22$  and  $y_t^2 = 0.28$ . For these values the pseudoscalar contribution yields less than one event. Thus  $H^0$  must account for all 20 events. We can thus use Eq. (2.11) which gives

$$c_\gamma > 4.1. \quad (3.36)$$

As explained below Eq. (3.33) the maximal possible value of  $c_\gamma$  is 3 when  $\lambda_{H^+} = 16\pi^2/\sqrt{3}$ . This yields only half of the required number of events according to the above bound. In any case such large values of  $\lambda_{H^+}$  are ruled out if we require the contribution of  $\lambda_{H^+}$  to the running of  $\lambda_V$  to be smaller than the electroweak precision bound, that is  $\Delta\lambda_V < 3$ . This rules out the quark-antiquark production as a possibility.

Thus, we have verified that the general 2HDM, without any additional states, cannot account for the observed anomaly.

### 3.3 The fate of the MSSM

We now turn to the Minimal Supersymmetric Standard Model (MSSM). As in the 2HDM, which in its type-II form is contained in the MSSM as a subsector, the only candidate particles for the resonance in the MSSM are  $H^0$  and  $A^0$ .<sup>3</sup> Again, the only viable production

<sup>3</sup> We consider the R-parity-conserving MSSM, otherwise in principle one could consider sneutrino candidates, which can be similarly constrained. A resonant  $\gamma\gamma$  signal can also arise within the MSSM from the annihilation of a squark-antisquark near-threshold QCD bound state, most famously the stoponium [36]. However, based on expressions from [37], the stoponium has  $|c_g c_\gamma| \simeq 2^{18} (\pi/3)^5 \zeta(3) \alpha \alpha_s \bar{\alpha}_s^3 \approx 0.7$ , so the rate is way too small to account for the excess if  $\Gamma = 45$  GeV (c.f. Eq. (2.9)). Even assuming the observed resonance to actually be narrow and taking the most favorable (but also a quite generic) scenario where the width is saturated by decays to the production mode,  $\Gamma_{gg} \simeq (16/81) \bar{\alpha}_s^3 \alpha_s^2 M \approx 0.0033$  GeV, the r.h.s. of Eq. (2.9) is still as large as 4.5. This is still too large by a factor of about 6. One might also consider the gluonium, whose production cross section is much larger, though the  $\gamma\gamma$  annihilation channel is loop-suppressed [37, 38]. However, pair production of  $M/2 = 375$  GeV gluinos would have been almost certainly noticed by now.

mode is from gluon fusion, due to small Yukawa couplings and the fact that we are deep in the decoupling regime,  $M_{H^0} \gg M_Z$ . As we have seen above, the 2HDM fails by a large margin to accommodate the data. However, in the MSSM there are extra contributions to the  $Hgg$  couplings from sfermions and to the  $H^0\gamma\gamma$  couplings from sfermions and charginos, in addition to those already present in the 2HDM. The  $A^0gg$  and  $A^0\gamma\gamma$  vertices receive no sfermion contributions at one loop as a consequence of CP symmetry, though they do receive contributions from charginos.<sup>4</sup> Dimensional analysis gives, for the contribution of the two stops, for  $M_{\text{SUSY}} = 1 \text{ TeV}$ ,

$$c_g \sim 2g_s^2 \times \frac{vM_{H^0}}{M_{\text{SUSY}}^2} \sim 0.5$$

and

$$c_\gamma \sim 2N_c e^2 \times \frac{vM_{H^0}}{M_{\text{SUSY}}^2} \sim 0.1.$$

Even allowing for similar contributions from other sparticles, this suggests that generically, the product  $|c_g c_\gamma| < 1$ , nearly three orders of magnitude below what is required according to Eq. (2.9). However, we must also contemplate that the true resonance width could be smaller than the “nominal” 45 GeV. The decay width of  $H^0$  is dominated by tree-level decays into top and bottom quarks, and is essentially determined in the MSSM as a function of  $\tan\beta$ , with a minimum of about 2 GeV at  $\tan\beta \approx 6$ . Hence, Eq. (2.9) can be recast as

$$\frac{|c_\gamma c_g|}{\sqrt{\Gamma(\tan\beta)/(45 \text{ GeV})}} = \rho_g \approx 530. \quad (3.37)$$

The question is how large the left-hand side may be. First, a small numerator could be partly compensated for by a factor of up to five due to the denominator. Second, an MSSM spectrum could also be quite non-degenerate, with hierarchies like  $m_{\tilde{t}_1} \ll M_{H^0}, \mu \ll m_{\tilde{t}_2}$ ; this is in fact favoured by the observed Higgs mass. In particular, large  $\mu$  and/or  $A$ -terms and a light stop can lead to a parametric enhancement  $\sim \{\mu, A_t\}/m_{\tilde{t}_1}$  relative to the naive estimates above. Third, there could also be important contributions from sbottoms and staus, as well as charginos, which brings in a large subset of the MSSM parameters. A conclusion about the fate of the MSSM requires a quantitative treatment, but a brute-force parameter scan is not really feasible and in any case beyond the scope of this work. Instead, the purpose of the rest of this section is to obtain simple yet conservative bounds on all one-loop contributions over the entire MSSM parameter space. First, we will be imposing  $\tan\beta > 1$ . The reason is that the  $H^0 t\bar{t}$  coupling is  $\sqrt{2}m_t/(v \tan\beta)$  in the decoupling limit, which for  $\tan\beta < 1$  implies a decay width significantly exceeds the width allowed by observations, cf section 2.1. (Independently, such large couplings would lead to a Landau pole in  $y_t$ , and/or strong coupling at low scales, and has very strong support from the observed Higgs mass of 125 GeV, which we will not separately impose.) The key assumption

<sup>4</sup>As in the rest of this work, we assume CP conservation. Without this assumption, the gluonic and photonic couplings of some superposition of the two heavier mass eigenstates  $H_2$  and  $H_3$  will receive sparticle loop contributions, so apart from a division of the diphoton signal between  $H_2$  and  $H_3$  resonant contributions, we do not expect qualitative changes to our conclusions.

will be the absence of charge- and colour-breaking minima of the scalar potential. This could in principle be relaxed to only require metastability over cosmological timescales; we leave this aside for future work. As we will see, this assumption is sufficient to exclude the MSSM if the resonance interpretation is confirmed.

### 3.3.1 Constraints from vacuum stability

An essential role in our argument is played by the upper bounds on the  $\mu$  parameter and the soft trilinear terms that follow from requiring the absence of charge- and colour-breaking minima of the MSSM scalar potential. The derivation of these bounds is well known [39–46] and involves suitable one-dimensional directions of the MSSM scalar field space. Employing the four directions

$$T_L = T_R = H_u^0, \quad B_L = B_R = H_d^0, \quad B_L = T_R = H_d^-, \quad T_L = B_R = H_u^+ \quad (3.38)$$

(with all other scalar fields held at zero), of which the first two are  $D$ -flat, the bounds following from the four can be conveniently formulated in terms of the stop and sbottom masses, as follows:

$$|A_t| \leq \sqrt{3} \sqrt{m_{t_1}^2 + m_{t_2}^2 - 2m_t^2 + \frac{M_{H^0}^2}{2} [1 + \cos(2\beta)] - \frac{m_Z^2}{2} \cos(2\beta)}, \quad (3.39)$$

$$|A_b| \leq \sqrt{3} \sqrt{m_{b_1}^2 + m_{b_2}^2 - 2m_b^2 + \frac{M_{H^0}^2}{2} [1 - \cos(2\beta)]}, \quad (3.40)$$

$$|\mu| \leq \sqrt{1 + \frac{m_Z^2}{m_t^2} \sin^2 \beta} \quad (3.41)$$

$$\begin{aligned} & \times \sqrt{m_{t_1}^2 + m_{t_2}^2 - 2m_t^2 + \frac{M_{H^0}^2}{2} [1 - \cos(2\beta)] - m_Z^2 \cos(2\beta)}, \\ m_b |\mu| \tan \beta & \leq m_t \sqrt{\frac{\tan^2 \beta}{R^2} + \frac{m_Z^2}{m_t^2} \sin^2 \beta} \quad (3.42) \\ & \times \sqrt{m_{b_1}^2 + m_{b_2}^2 - 2m_b^2 + \frac{M_{H^0}^2}{2} [1 + \cos(2\beta)] + \frac{m_Z^2}{2} \cos(2\beta)}, \end{aligned}$$

where  $R = m_t/m_b \sim 50$ . The second and fourth bounds hold, upon substituting  $b \rightarrow \tau$ , for the stau sector, as well. No simplifications have been made. The first bound sometimes has no solution; this means that the corresponding very small stop mass values are excluded on theoretical grounds. We can combine the bounds into bounding functions  $\Phi_t$ ,  $\Phi_b$ , and  $\Phi_\tau$  of the sfermion masses and  $\beta$  only. Firstly,

$$\Phi_t = \begin{cases} 0, & m_{t_1}^2 + m_{t_2}^2 - 2m_t^2 + \frac{M_{H^0}^2}{2} [1 + \cos(2\beta)] - \frac{m_Z^2}{2} \cos(2\beta) < 0, \\ \sqrt{3} \sqrt{m_{t_1}^2 + m_{t_2}^2 - 2m_t^2 + \frac{M_{H^0}^2}{2} [1 - \cos(2\beta)] - m_Z^2 \cos(2\beta)}, & \text{otherwise.} \end{cases} \quad (3.43)$$

If the condition for  $\Phi_t = 0$  is satisfied, there is no way to satisfy the  $A_t$  constraint; setting the bounding function to zero in this case will serve to effectively discard those unphysical

points below. Otherwise,  $\Phi_t$  simultaneously bounds both  $|A_t|$  and  $|\mu|$ . A similar function that simultaneously bounds  $|A_b|$  and  $\frac{m_b}{m_t}|\mu| \tan \beta$  is provided by

$$\Phi_b = \sqrt{3} \sqrt{m_{b_1}^2 + m_{b_2}^2 - 2m_b^2 + \frac{M_{H^0}^2}{2}[1 - \cos(2\beta)]}, \quad (3.44)$$

and an identical function  $\Phi_\tau$  follows from this upon substituting  $b \rightarrow \tau$ .

### 3.3.2 Conservative bounds on sfermion contributions

In the notation of [47], the sfermion contributions to  $c_g$  are given by

$$\left| \sum_f c_g^{(\tilde{f})} \right| = \frac{g M_{H^0}}{2 M_W} g_s^2 \left| A_{\text{SUSY}, \tilde{f}}^{H^0} \right|. \quad (3.45)$$

If the contribution of a sfermion to  $c_g$  is known, the corresponding contribution to  $c_\gamma$  is given by

$$c_\gamma^{(\tilde{f})} = 2(e^2/g_s^2) N_c^{(f)} Q_f^2 c_g^{(\tilde{f})}. \quad (3.46)$$

Explicitly,

$$A_{\text{SUSY}, \tilde{f}}^{H^0} = 4 \sum_{\tilde{f}=\tilde{t}, \tilde{b}, \tilde{\tau}} \sum_{i=1,2} \frac{g_{\tilde{f}_i \tilde{f}_i}^{H^0}}{M_{H^0}^2} h(\tau_i^{\tilde{f}}) \quad (3.47)$$

where  $\tau_i^{\tilde{f}} = M_{H^0}^2/(4m_{\tilde{f}_i}^2)$  and

$$h(\tau) = \tau A_0^{H^0}(\tau) = \begin{cases} \frac{\arcsin^2(\sqrt{\tau})}{\tau} - 1 & \tau \leq 1, \\ -\frac{1}{4\tau} \left( \ln \frac{1 + \sqrt{1 - \frac{1}{\tau}}}{1 - \sqrt{1 - \frac{1}{\tau}}} - i\pi \right)^2 - 1 & \tau > 1. \end{cases} \quad (3.48)$$

Consider first the stops. In the decoupling limit, their couplings to  $H^0$  are

$$g_{\tilde{t}_i \tilde{t}_i}^{H^0} = -\cot \beta m_{\tilde{t}_i}^2 + x_i \sin(2\beta) M_Z^2 \pm m_t \frac{\sin(2\theta_{\tilde{t}_i})}{2} (\mu + A_t \cot \beta), \quad (3.49)$$

where  $\theta_{\tilde{t}_i}$  is the stop mixing angle, and the coefficients  $x_i$  depend on  $\theta_{\tilde{t}_i}$  and  $\beta$  and are always less than one in magnitude. Using that  $h \rightarrow 0$  for  $\tau \rightarrow 0, \infty$  and  $|h| \leq h(1) \approx 1.47$ , one easily shows that the first two terms lead to maximal contributions to  $A_{\text{SUSY}, \tilde{f}}^{H^0}$  that are bounded (in magnitude) by  $2.74 \cot \beta$  and  $0.03$ , respectively. (Similar terms for the sbottom and stau cases will be negligible.) The third term in the coupling leads to

$$A_{\text{SUSY}, \tilde{t}}^{H^0} = \frac{\sin(2\theta_{\tilde{t}_i})}{2} \frac{4 m_t (A_t \cot \beta + \mu)}{M_{H^0}^2} \times (h(\tau_1) - h(\tau_2)). \quad (3.50)$$

Employing now the bounding function  $\Phi_t$  from the previous subsection, it is not difficult to show that

$$\left| m_t \frac{\sin(2\theta_{\tilde{t}_i})}{2} (A_t \cot \beta + \mu) \right| \leq m_t \min \left( \frac{1}{2} \Phi_t (1 + \cot \beta), m_t \frac{\Phi_t^2}{m_{\tilde{t}_2}^2 - m_{\tilde{t}_1}^2} \right) \equiv \frac{M_{H^0}^2}{4} B(\tau_1, \tau_2; M_{H^0}). \quad (3.51)$$

The first argument of the min function follows from  $|\sin| \leq 1$ , the second makes use of the explicit formula for the stop mixing angle. We then have

$$|A_{\text{SUSY},\tilde{t}}^{H^0}| \leq B(\tau_1, \tau_2) |h(\tau_1) - h(\tau_2)|. \quad (3.52)$$

The right-hand side is bounded and the physical parameter space is the compact region  $0 \leq \tau_i \leq \tau_i^{\text{max}}$ , where  $\tau_i^{\text{max}} = M_{H^0}^2 / (4m_{\tilde{t}}^{\text{min}})$  depends on the experimental lower bound on the lighter stop mass. Straightforward numerical techniques establish that

$$|A_{\text{SUSY},\tilde{t}}^{H^0}| \leq 3.37, \quad (3.53)$$

where the maximum is obtained at  $\tan \beta = 1$ , when one stop is at threshold ( $m = M_H/2$ ) and the other is relatively light. Below, we numerically obtain and use the bounds as a function of  $\tan \beta$ . (We allow stop masses as light as 100 GeV in the scan, to escape any doubts related to for instance compressed spectra where light stops might have escaped detection at the LHC). The extremal point is generally ruled out by the observed Higgs mass  $m_h = 125$  GeV, and very unlikely to be consistent with LHC searches, but we are being conservative.

Analogous steps lead to bounds on the sbottom and stau contributions. In this case, terms proportional to  $m_{b,\tau}^2$  and  $m_Z^2$  in the Higgs-sfermion couplings lead to completely negligible effects. For the remainder, we require a bound

$$\begin{aligned} \left| m_b \frac{\sin(2\theta_{\tilde{b}})}{2} (\mu - A_b \tan \beta) \right| &\leq m_t \min \left( \frac{1}{2} M_b \left[ \cot \beta + \frac{\tan \beta}{R} \right], \right. \\ &\quad \left. m_t \frac{M_b^2}{m_{\tilde{b}_2}^2 - m_{\tilde{b}_1}^2} \left[ \cot \beta + \frac{\tan \beta}{R} \right] \left[ 1 + \frac{1}{R} \right] \right) \\ &\equiv \frac{M_{H^0}^2}{4} B_{\tilde{b}}(\tau_1, \tau_2; M_{H^0}). \end{aligned} \quad (3.54)$$

The resulting bound is most effective in the intermediate  $\tan \beta$  region, counteracting the small denominator of Eq. (3.37) in that region. The bound on the stau contribution, as a function of  $\tan \beta$  and the slepton masses, is identical to the sbottom one, except for a missing colour factor (overcompensated in the photonic coupling by a ninefold larger squared electric charge).

### 3.3.3 Contributions from other particles and verdict

The contributions from top, bottom,  $W$ , and charged-Higgs loops have already been discussed in the 2HDM section. In the decoupling limit, where  $M_{H^+} \approx M_{H^0}$ , they are essentially functions of  $\tan \beta$  only and easily incorporated. Regarding charginos, their effect is equivalent to the contribution of two vectorlike, colourless particles; such contributions have also been discussed above. We only need to bound the fermion loop function by its global maximum and make no use of the relation of the chargino and Higgs mixing angles to MSSM parameters in order to obtain the bound  $|c_\gamma^{\chi^\pm}| \leq 0.45$  (for any  $\tan \beta$ ). Assuming now the extreme scenario where all contributions to  $c_\gamma$  and  $c_g$  simultaneously saturate their bounds and are in phase with one another, we obtain a (very) conservative upper

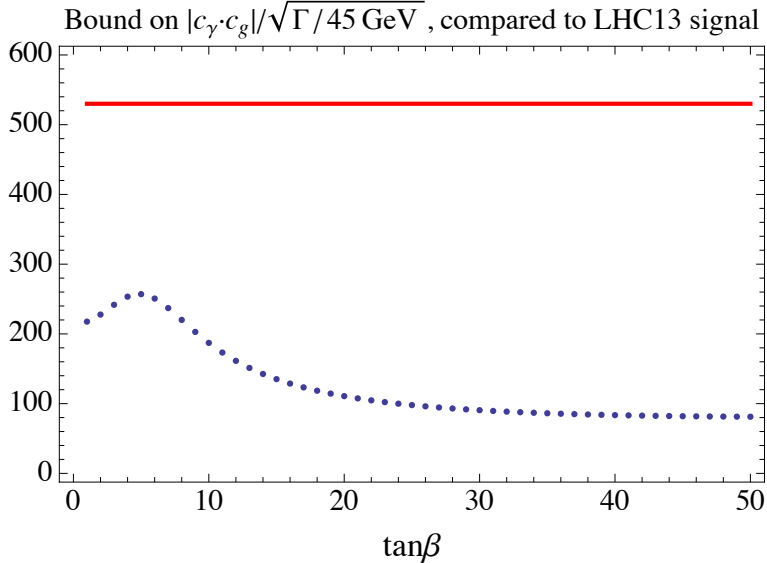


**Figure 8.** Comparison of the upper bound on the left-hand side of Eq. (3.37) to the signal suggested by the diphoton excesses, as a function of  $\tan\beta$ . The red horizontal line corresponds to the signal, and the blue dots represent our conservative upper bound.

bound on the left-hand side of Eq. (3.37). This is displayed in Figure 8. We observe that this bound still misses the data by more than a factor of two, even at the point of closest approach at  $\tan\beta \sim 5$ . It is fairly clear that the bound could be made stronger by, for example, employing more properties of the function  $h$  or formulating a higher-dimensional extremization problem (closer to a full scan of the MSSM parameter space). We must also stress that our conclusions here are specific to the MSSM, and attest to the high predictivity of the model. If the MSSM cannot survive in regions of metastability (where charge and colour-breaking minima exist but are not tunneled to over cosmological timescales, an unlikely possibility), more complicated supersymmetric models might hence still accommodate the excess, although the techniques described here may be useful in scrutinizing them. Another logical possibility of saving the MSSM would be production through the decay of heavier particles (say, stops, which could themselves be produced from gluino and squark decays). As mentioned in the beginning, the experimental data do not seem to support such a mechanism.

## 4 Summary and Outlook

This work deals with the core phenomenology of the diphoton excess observed by the LHC experiments ATLAS and CMS around 750 GeV diphoton invariant mass. We have considered both the case where the data are interpreted by a narrow and a broad resonance. We obtained model-independent constraints on the allowed couplings and branching fractions to various final states, including the interplay with other existing bounds. Our findings suggest that the anomaly cannot be accounted for by the presence of a single additional singlet or doublet spin-zero field and the Standard Model degrees of freedom; this includes

all two-Higgs-doublet models. We have proven that the whole parameter space of the MSSM is ruled out as an explanation for the excess if one requires the absence of charge and colour breaking minima. If we assume that the resonance is broad, we find that it is challenging to find a weakly coupled explanation. However, we provide an existence proof in the form of a model with vectorlike quarks with exotic electric charge of  $5/3$  or above. For the narrow resonance case, a similar model can be perturbative up to high scales also with smaller charges. We have also considered dilaton models, and they appear to be challenged by the data, even if arbitrary extra contributions to the QED and QCD beta functions are allowed. As already mentioned, in all the scenarios studied by us we find that new particles below the TeV scale need to be present in addition to the resonance. They must have couplings to the scalar itself, to photons and to gluons and possibly also to light quarks. Further study of their LHC phenomenology would be interesting to follow. Based on our toy models, in which the new resonance can have significant couplings to the light quarks, an interesting linkage between flavor physics and the physics related to the resonance may be present.

**Note:** Other early-response studies of the various possible implications of the excess, that appeared approximately simultaneously with ours, are Refs. [48–64]. Also, after the submission, an earlier study of diphoton resonances [65] was pointed out to us.

## Acknowledgments

GP is supported by the BSF, ISF, and ERC-2013-CoG grant (TOPCHARM # 614794). SJ thanks GP and the Weizmann Institute for hospitality, including the period during which this paper was conceived. SJ acknowledges partial support from the UK STFC under Grant Agreement ST/L000504/1, and from the IPPP through an associateship. SJ acknowledges the NExT Institute.

## References

- [1] ATLAS Collaboration, “Search for resonances decaying to photon pairs in  $3.2 \text{ fb}^{-1}$  of  $pp$  collisions at  $\sqrt{s} = 13 \text{ TeV}$  with the ATLAS detector,” Tech. Rep. ATLAS-CONF-2015-081, CERN, Geneva, 2015. <http://cds.cern.ch/record/2114853>.
- [2] CMS Collaboration, “Search for new physics in high mass diphoton events in proton-proton collisions at 13 TeV,” Tech. Rep. CMS-PAS-EXO-15-004, CERN, Geneva, 2015. <http://cds.cern.ch/record/2114808>.
- [3] L. D. Landau, “On the angular momentum of a system of two photons,” *Dokl. Akad. Nauk Ser. Fiz.* **60** (1948) 207.
- [4] C.-N. Yang, “Selection Rules for the Dematerialization of a Particle Into Two Photons,” *Phys. Rev.* **77** (1950) 242.
- [5] J. Alwall, R. Frederix, S. Frixione, V. Hirschi, F. Maltoni, O. Mattelaer, H.-S. Shao, T. Stelzer, P. Torrielli, and M. Zaro, “The automated computation of tree-level and next-to-leading order differential cross sections, and their matching to parton shower simulations,” *JHEP* **1407** (2014) 079, [arXiv:1405.0301](https://arxiv.org/abs/1405.0301) [[hep-ph](https://arxiv.org/archive/hep)].

- [6] S. Dawson, “The Effective  $W$  Approximation,” *Nucl. Phys.* **B249** (1985) 42.
- [7] G. L. Kane, W. W. Repko, and W. B. Rolnick, “The Effective  $W^\pm$ ,  $Z^0$  Approximation for High-Energy Collisions,” *Phys. Lett.* **B148** (1984) 367.
- [8] W. Altmannshofer, J. Galloway, S. Gori, A. L. Kagan, A. Martin, and J. Zupan, “On the 750 GeV di-photon excess,” [arXiv:1512.07616](https://arxiv.org/abs/1512.07616) [[hep-ph](#)].
- [9] R. D. Ball *et al.*, “Parton distributions with LHC data,” *Nucl. Phys.* **B867** (2013) 244, [arXiv:1207.1303](https://arxiv.org/abs/1207.1303) [[hep-ph](#)].
- [10] CMS Collaboration, V. Khachatryan *et al.*, “Search for diphoton resonances in the mass range from 150 to 850 GeV in pp collisions at  $\sqrt{s} = 8$  TeV,” *Phys. Lett.* **B750** (2015) 494, [arXiv:1506.02301](https://arxiv.org/abs/1506.02301) [[hep-ex](#)].
- [11] ATLAS Collaboration, G. Aad *et al.*, “Search for high-mass diphoton resonances in  $pp$  collisions at  $\sqrt{s} = 8$  TeV with the ATLAS detector,” *Phys. Rev.* **D92** (2015) 032004, [arXiv:1504.05511](https://arxiv.org/abs/1504.05511) [[hep-ex](#)].
- [12] CMS Collaboration, “Search for High-Mass Diphoton Resonances in pp Collisions at  $\sqrt{s} = 8$  TeV with the CMS Detector,” Tech. Rep. CMS-PAS-EXO-12-045, CERN, Geneva, 2015. <http://cds.cern.ch/record/2017806>.
- [13] CMS Collaboration, “Search for Resonances Decaying to Dijet Final States at  $\sqrt{s} = 8$  TeV with Scouting Data,” Tech. Rep. CMS-PAS-EXO-14-005, CERN, Geneva, 2015. <http://cds.cern.ch/record/2063491>.
- [14] CMS Collaboration, V. Khachatryan *et al.*, “Search for Resonant  $t\bar{t}$  Production in Proton-Proton Collisions at  $\sqrt{s} = 8$  TeV,” [arXiv:1506.03062](https://arxiv.org/abs/1506.03062) [[hep-ex](#)].
- [15] ATLAS Collaboration, G. Aad *et al.*, “Search for a high-mass Higgs boson decaying to a  $W$  boson pair in  $pp$  collisions at  $\sqrt{s} = 8$  TeV with the ATLAS detector,” [arXiv:1509.00389](https://arxiv.org/abs/1509.00389) [[hep-ex](#)].
- [16] CMS Collaboration, “Search for a standard model like Higgs boson in the  $H \rightarrow ZZ \rightarrow \ell^+ \ell^- q\bar{q}$  decay channel at  $\sqrt{s} = 8$  TeV,” Tech. Rep. CMS-PAS-HIG-14-007, CERN, Geneva, 2015. <https://cds.cern.ch/record/2001558>.
- [17] CMS Collaboration, “Search for di-Higgs resonances decaying to 4 bottom quarks,” Tech. Rep. CMS-PAS-HIG-14-013, CERN, Geneva, 2014. <http://cds.cern.ch/record/1748425>.
- [18] ATLAS Collaboration, G. Aad *et al.*, “Search for a new resonance decaying to a  $W$  or  $Z$  boson and a Higgs boson in the  $\ell\ell/\ell\nu/\nu\nu + b\bar{b}$  final states with the ATLAS detector,” *Eur. Phys. J.* **C75** (2015) 263, [arXiv:1503.08089](https://arxiv.org/abs/1503.08089) [[hep-ex](#)].
- [19] ATLAS Collaboration, G. Aad *et al.*, “Search for neutral Higgs bosons of the minimal supersymmetric standard model in  $pp$  collisions at  $\sqrt{s} = 8$  TeV with the ATLAS detector,” *JHEP* **11** (2014) 056, [arXiv:1409.6064](https://arxiv.org/abs/1409.6064) [[hep-ex](#)].
- [20] ATLAS Collaboration, G. Aad *et al.*, “Search for new resonances in  $W\gamma$  and  $Z\gamma$  final states in  $pp$  collisions at  $\sqrt{s} = 8$  TeV with the ATLAS detector,” *Phys. Lett.* **B738** (2014) 428, [arXiv:1407.8150](https://arxiv.org/abs/1407.8150) [[hep-ex](#)].
- [21] ATLAS Collaboration, G. Aad *et al.*, “Search for high-mass dilepton resonances in  $pp$  collisions at  $\sqrt{s} = 8$  TeV with the ATLAS detector,” *Phys. Rev.* **D90** (2014) 052005, [arXiv:1405.4123](https://arxiv.org/abs/1405.4123) [[hep-ex](#)].
- [22] CMS Collaboration, S. Chatrchyan *et al.*, “Search for narrow resonances and quantum black

- holes in inclusive and  $b$ -tagged dijet mass spectra from  $pp$  collisions at  $\sqrt{s} = 7$  TeV,” *JHEP* **01** (2013) 013, [arXiv:1210.2387 \[hep-ex\]](#).
- [23] CMS Collaboration, “Search for Heavy Resonances Decaying into  $b\bar{b}$  and  $bg$  Final States in  $pp$  Collisions at  $\sqrt{s} = 8$  TeV,” Tech. Rep. CMS-PAS-EXO-12-023, CERN, Geneva, 2013. <http://cds.cern.ch/record/1542405>.
- [24] ATLAS Collaboration, “Search for New Phenomena in Dijet Mass and Angular Distributions from  $pp$  Collisions at  $\sqrt{s} = 13$  TeV with the ATLAS Detector,” [arXiv:1512.01530 \[hep-ex\]](#).
- [25] CMS Collaboration, V. Khachatryan *et al.*, “Search for narrow resonances decaying to dijets in proton-proton collisions at  $\sqrt{s} = 13$  TeV,” [arXiv:1512.01224 \[hep-ex\]](#).
- [26] W. D. Goldberger, B. Grinstein, and W. Skiba, “Distinguishing the Higgs boson from the dilaton at the Large Hadron Collider,” *Phys. Rev. Lett.* **100** (2008) 111802, [arXiv:0708.1463 \[hep-ph\]](#).
- [27] T. Robens and T. Stefaniak, “Status of the Higgs Singlet Extension of the Standard Model after LHC Run 1,” *Eur. Phys. J.* **C75** (2015) 104, [arXiv:1501.02234 \[hep-ph\]](#).
- [28] M. Spira, A. Djouadi, D. Graudenz, and P. M. Zerwas, “Higgs boson production at the LHC,” *Nucl. Phys.* **B453** (1995) 17, [arXiv:hep-ph/9504378](#).
- [29] A. Efrati, E. Kuflik, S. Nussinov, Y. Soreq, and T. Volansky, “Constraining the Higgs-Dilaton with LHC and Dark Matter Searches,” *Phys. Rev.* **D91** (2015) 055034, [arXiv:1410.2225 \[hep-ph\]](#).
- [30] B. Bellazzini, C. Csaki, J. Hubisz, J. Serra, and J. Terning, “A Higgslike Dilaton,” *Eur. Phys. J.* **C73** (2013) 2333, [arXiv:1209.3299 \[hep-ph\]](#).
- [31] B. Gripaios, A. Pomarol, F. Riva, and J. Serra, “Beyond the Minimal Composite Higgs Model,” *JHEP* **04** (2009) 070, [arXiv:0902.1483 \[hep-ph\]](#).
- [32] G. C. Branco, L. Lavoura, and J. P. Silva, “CP Violation,” *Int. Ser. Monogr. Phys.* **103** (1999) 1.
- [33] R. S. Gupta, M. Montull, and F. Riva, “SUSY Faces its Higgs Couplings,” *JHEP* **04** (2013) 132, [arXiv:1212.5240 \[hep-ph\]](#).
- [34] J. F. Gunion and H. E. Haber, “The CP conserving two Higgs doublet model: The Approach to the decoupling limit,” *Phys. Rev.* **D67** (2003) 075019, [arXiv:hep-ph/0207010](#).
- [35] D. Ghosh, R. S. Gupta, and G. Perez, “Is the Higgs Mechanism of Fermion Mass Generation a Fact? A Yukawa-less First-Two-Generation Model,” [arXiv:1508.01501 \[hep-ph\]](#).
- [36] M. Drees and M. M. Nojiri, “Proposed new signal for scalar top-squark bound-state production,” *Phys. Rev. Lett.* **72** (1994) 2324, [arXiv:hep-ph/9310209](#).
- [37] D. Kahawala and Y. Kats, “Distinguishing spins at the LHC using bound state signals,” *JHEP* **09** (2011) 099, [arXiv:1103.3503 \[hep-ph\]](#).
- [38] M. R. Kauth, J. H. Kuhn, P. Marquard, and M. Steinhauser, “Gluinonia: Energy Levels, Production and Decay,” *Nucl. Phys.* **B831** (2010) 285, [arXiv:0910.2612 \[hep-ph\]](#).
- [39] J. M. Frere, D. R. T. Jones, and S. Raby, “Fermion Masses and Induction of the Weak Scale by Supergravity,” *Nucl. Phys.* **B222** (1983) 11.
- [40] J. P. Derendinger and C. A. Savoy, “Quantum Effects and  $SU(2) \times U(1)$  Breaking in

- Supergravity Gauge Theories,” *Nucl. Phys.* **B237** (1984) 307.
- [41] J. A. Casas and S. Dimopoulos, “Stability bounds on flavor violating trilinear soft terms in the MSSM,” *Phys. Lett.* **B387** (1996) 107, [arXiv:hep-ph/9606237](#).
- [42] R. Rattazzi and U. Sarid, “The Unified minimal supersymmetric model with large Yukawa couplings,” *Phys. Rev.* **D53** (1996) 1553, [arXiv:hep-ph/9505428](#).
- [43] J. Hisano and S. Sugiyama, “Charge-breaking constraints on left-right mixing of stau’s,” *Phys. Lett.* **B696** (2011) 92, [arXiv:1011.0260 \[hep-ph\]](#). [Erratum: *Phys. Lett.* **B719** (2013) 472].
- [44] W. Altmannshofer, M. Carena, N. R. Shah, and F. Yu, “Indirect Probes of the MSSM after the Higgs Discovery,” *JHEP* **01** (2013) 160, [arXiv:1211.1976 \[hep-ph\]](#).
- [45] M. Carena, S. Gori, I. Low, N. R. Shah, and C. E. M. Wagner, “Vacuum Stability and Higgs Diphoton Decays in the MSSM,” *JHEP* **02** (2013) 114, [arXiv:1211.6136 \[hep-ph\]](#).
- [46] W. Altmannshofer, C. Frugiuele, and R. Harnik, “Fermion Hierarchy from Sfermion Anarchy,” *JHEP* **12** (2014) 180, [arXiv:1409.2522 \[hep-ph\]](#).
- [47] A. Djouadi, “The Anatomy of electro-weak symmetry breaking. II. The Higgs bosons in the minimal supersymmetric model,” *Phys. Rept.* **459** (2008) 1, [arXiv:hep-ph/0503173](#).
- [48] K. Harigaya and Y. Nomura, “Composite Models for the 750 GeV Diphoton Excess,” [arXiv:1512.04850 \[hep-ph\]](#).
- [49] Y. Mambrini, G. Arcadi, and A. Djouadi, “The LHC diphoton resonance and dark matter,” [arXiv:1512.04913 \[hep-ph\]](#).
- [50] M. Backovic, A. Mariotti, and D. Redigolo, “Di-photon excess illuminates Dark Matter,” [arXiv:1512.04917 \[hep-ph\]](#).
- [51] A. Angelescu, A. Djouadi, and G. Moreau, “Scenarii for interpretations of the LHC diphoton excess: two Higgs doublets and vector-like quarks and leptons,” [arXiv:1512.04921 \[hep-ph\]](#).
- [52] Y. Nakai, R. Sato, and K. Tobioka, “Footprints of New Strong Dynamics via Anomaly,” [arXiv:1512.04924 \[hep-ph\]](#).
- [53] S. Knapen, T. Melia, M. Papucci, and K. Zurek, “Rays of light from the LHC,” [arXiv:1512.04928 \[hep-ph\]](#).
- [54] D. Buttazzo, A. Greljo, and D. Marzocca, “Knocking on New Physics’ door with a Scalar Resonance,” [arXiv:1512.04929 \[hep-ph\]](#).
- [55] A. Pilaftsis, “Diphoton Signatures from Heavy Axion Decays at LHC,” [arXiv:1512.04931 \[hep-ph\]](#).
- [56] R. Franceschini, G. F. Giudice, J. F. Kamenik, M. McCullough, A. Pomarol, R. Rattazzi, M. Redi, F. Riva, A. Strumia, and R. Torre, “What is the  $\gamma\gamma$  resonance at 750 GeV?,” [arXiv:1512.04933 \[hep-ph\]](#).
- [57] S. Di Chiara, L. Marzola, and M. Raidal, “First interpretation of the 750 GeV di-photon resonance at the LHC,” [arXiv:1512.04939 \[hep-ph\]](#).
- [58] T. Higaki, K. S. Jeong, N. Kitajima, and F. Takahashi, “The QCD Axion from Aligned Axions and Diphoton Excess,” [arXiv:1512.05295 \[hep-ph\]](#).
- [59] S. D. McDermott, P. Meade, and H. Ramani, “Singlet Scalar Resonances and the Diphoton

- Excess,” [arXiv:1512.05326 \[hep-ph\]](#).
- [60] J. Ellis, S. A. R. Ellis, J. Quevillon, V. Sanz, and T. You, “On the Interpretation of a Possible  $\sim 750$  GeV Particle Decaying into  $\gamma\gamma$ ,” [arXiv:1512.05327 \[hep-ph\]](#).
  - [61] M. Low, A. Tesi, and L.-T. Wang, “A pseudoscalar decaying to photon pairs in the early LHC run 2 data,” [arXiv:1512.05328 \[hep-ph\]](#).
  - [62] B. Bellazzini, R. Franceschini, F. Sala, and J. Serra, “Goldstones in Diphotons,” [arXiv:1512.05330 \[hep-ph\]](#).
  - [63] C. Petersson and R. Torre, “The 750 GeV diphoton excess from the goldstino superpartner,” [arXiv:1512.05333 \[hep-ph\]](#).
  - [64] E. Molinaro, F. Sannino, and N. Vignaroli, “Strong dynamics or axion origin of the diphoton excess,” [arXiv:1512.05334 \[hep-ph\]](#).
  - [65] J. Jaeckel, M. Jankowiak, and M. Spannowsky, “LHC probes the hidden sector,” *Phys. Dark Univ.* **2** (2013) 111, [arXiv:1212.3620 \[hep-ph\]](#).